AFRL-SR-AR-TR-04-

0515

REPORT DOCUMENTATION PAGE

The public reporting burden for this collection of information is estimated to average 1 hour per response, including gathering and maintaining the data needed, and completing and reviewing the collection of information. Send comments regarding this bu...... of information, including suggestions for reducing the burden, to Department of Defense, Washington Headquarters Services, Directorate for Informatio..... (0704-0188), 1215 Jefferson Davis Highway, Suite 1204, Arlington, VA 22202-4302. Respondents should be aware that notwithstanding any other provision of law, no person shall be subject to any penalty for failing to comply with a collection of information if it does not display a currently valid OMB control number.
PLEASE DO NOT RETURN YOUR FORM TO THE ABOVE ADDRESS.

1. REPORT DATE *(DD-MM-YYYY)*	2. REPORT TYPE	3. DATES COVERED *(From - To)*
24-09-2004	Final Performance Report	01-04-2001 - 30-06-2004

4. TITLE AND SUBTITLE	5a. CONTRACT NUMBER
Dielectric Non-Destructive Analysis of Adhesive Bonded Structures	
	5b. GRANT NUMBER F49620-01-1-0320
	5c. PROGRAM ELEMENT NUMBER

6. AUTHOR(S)	5d. PROJECT NUMBER
Mijovic, Jovan	
	5e. TASK NUMBER
	5f. WORK UNIT NUMBER

7. PERFORMING ORGANIZATION NAME(S) AND ADDRESS(ES)	8. PERFORMING ORGANIZATION REPORT NUMBER
Polytechnic University Six Metrotech Center Brooklyn, NY 11201	

9. SPONSORING/MONITORING AGENCY NAME(S) AND ADDRESS(ES)	10. SPONSOR/MONITOR'S ACRONYM(S)
Air Force Office of Scientific Research 801 N. Randolph St., Room 732 Arlington, VA 22230 NL	AFOSR
	11. SPONSOR/MONITOR'S REPORT NUMBER(S)

12. DISTRIBUTION/AVAILABILITY STATEMENT

Approve for Public Release: Distribution Unlimited

20041021 051

13. SUPPLEMENTARY NOTES

14. ABSTRACT

An investigation was conducted aimed at developing dielectric spectroscopy as a non-destructive inspection tool to asses aging of adhesive bonded structures. Dielectric spectroscopy was found to be a sensitive tool capable of detecting defects and absorbed moisture in adhesive bonded structures. The highlights of the research performed are:1) The defects in adhesive joints decrease the real and imaginary dielectric permittivity in the frequency domain and induce additional peaks in the time domain spectra;2) The dielectric spectra of dry epoxy-amine networks are characterized by two Arrhenius-like local relaxations: the beta process, associated with hydroxyl groups and the gamma process, associated with primary and secondary amine, and glycidyl ether groups; 3) Dynamics of beta and gamma processes are affected by short time aging. New relaxation processes appear in both model and commercial epoxy-amine adhesives after long term exposure to moisture. 4) Time domain reflectometry (TDR) traces shift to longer time with water ingress in the early stages of aging, but this trend is reversed at some critical time, which is possibly a signature of disbonding.

15. SUBJECT TERMS

Adhesive Joints, Non-Destructive Inspection, Dielectric Spectroscopy

16. SECURITY CLASSIFICATION OF:			17. LIMITATION OF ABSTRACT	18. NUMBER OF PAGES	19a. NAME OF RESPONSIBLE PERSON
a. REPORT	b. ABSTRACT	c. THIS PAGE	SAR	146	Mijovic Jovan
U	U	U			**19b. TELEPHONE NUMBER** *(Include area code)* 718-260-3097

Standard Form 298 (Rev. 8/98)
Prescribed by ANSI Std. Z39.18

FINAL PERFORMANCE REPORT

Grant No. F49620-01-1-0320

Dielectric Non-Destructive Analysis of Adhesive Bonded Structures

Dr. Jovan Mijovic
Othmer Department of Chemical and Biological Sciences and Engineering
Polytechnic University
Six Metrotech Center
Brooklyn, NY 11201
jmijovic@poly.edu

September 28, 2004

ABSTRACT

An investigation was conducted aimed at developing dielectric spectroscopy as a non-destructive inspection tool to asses aging of adhesive bonded structures. Dielectric spectroscopy was found to be a sensitive tool capable of detecting defects and absorbed moisture in adhesive bonded structures. The highlights of the research performed are:

1) The defects in adhesive joints decrease the real and imaginary dielectric permittivity in the frequency domain and induce additional peaks in the time domain spectra;

2) The dielectric spectra of dry epoxy-amine networks are characterized by two Arrhenius-like local relaxations: the β process, associated with hydroxyl groups and the γ process, associated with primary and secondary amine, and glycidyl ether groups;

3) Dynamics of β and γ processes are affected by short time aging. New relaxation processes appear in both model and commercial epoxy–amine adhesives after long term exposure to moisture.

4) Time domain reflectometry (TDR) traces shift to longer time with water ingress in the early stages of aging, but this trend is reversed at some critical time. The time at which the shift is observed is possibly a signature of disbonding.

5) Molecular-level explanation of water-network interaction in adhesive joints was obtained from FTIR and molecular dynamics simulation.

Table of Contents

List of Figures

List of Tables

List of Equations

2 Objectives

The principal objective of this research is to develop dielectric spectroscopy as a non-destructive inspection (NDI) tool to asses aging of adhesive bonded structures. The specific objectives are described under Statement of Objectives in the original proposal and have not been changed except for the addition of molecular dynamics simulation to the gamut of techniques already in use.

3 Status of Effort

The highlights of our research are as follows:

6) The effects of defects had been investigated by both frequency domain and time domain dielectric spectroscopy: we found that the defects decrease both the real and imaginary parts of dielectric permittivity in the frequency domain and induce extra peaks in the time domain spectra;

7) The DRS study of the dry epoxy-amine networks shows that those networks are characterized by two Arrhenius-like local relaxations: the β process, associated with hydroxyl groups and the γ process, associated with primary and secondary amine, and glycidyl ether groups;[1]

8) During short time aging, the absorbed water interacts with the network and affects the dynamics of β and γ processes;[1] after long time exposure, new processes appear in both model epoxy –amine (DGEBA-DETA) adhesives and commercial (Epibond 1590 from Vantico Adhesives) adhesives;

9) In the early stages of aging, the time domain reflectometry (TDR) traces shift to longer time with water ingress. After some critical time, the TDR traces reverse their trend and shift to shorter time. This is likely caused by disbonding;

10) Attempts at embedding optical fibers in the adhesive were not entirely satisfactory and efforts along those lines are continuing;

11) Molecular dynamics simulation study has yielded interesting results and could further our fundamental understanding of this issue.[2]

4 Accomplishments

This project's main goal was to develop dielectric spectroscopy as a non-destructive inspection (NDI) tool to asses the states of adhesive bonded structures. For freshly made joints, we found that dielectric spectra are sensitive to defects. During water exposure, dielectric spectra change with exposure time and/or water content. These observations show the suitability of dielectric spectroscopy as an NDI tool to asses the state of adhesive bonded structures.

The presentation of our results is organized as follows. We start with freshly made joints, where the effects of defects were studied using both frequency domain and time domain dielectric spectroscopy (section 4.1). Next, we move on to the effect of water exposure (section 4.2). In this part we describe the results of the frequency domain dielectric relaxation spectroscopy (DRS) (4.2.1), Time Domain Reflectometry (TDR) (4.2.2), fiber- optic near infrared spectroscopy (4.2.3), and Molecular Dynamics simulation (MD) (4.2.4). During this project, we also worked on the optimization of testing equipment and those efforts are described in section 4.3.

4.1 Effect of Defects

There are many types of flaws that can exist or develop in the adhesive or at the adhesive-adherend interface. Such flaws can vary from the molecular-level alterations to visible cracks, caused by manufacturing or preparation errors, or resulting from the service in harsh environments. Such defects damage the adhesive system in different ways, but the loss of mechanical strength is of greatest concern. We studied the effect of defects using frequency domain Dielectric Relaxation Spectroscopy (DRS) (4.1.1) and Time Domain Reflectometry (TDR) (4.1.2).

4.1.1 Frequency Domain Dielectric Relaxation Spectroscopy (DRS)

Experimental

Materials: Defects were simulated by placing Teflon patches in adhesive joints, as shown in Figure 4.1.1.1. A two component epoxy-amine (diglycidylether of bisphenol A, DGEBA, and diethylene triamine, DETA) formulation was used. DGEBA and DETA (their chemical formulae are shown in Figure 4.1.1.2) were obtained from Aldrich Chemical Company and were used as received. The two liquid components were mixed and stirred continuously until a clear, homogeneous mixture was obtained. A typical cure schedule consisted of keeping the as-mixed sample for 12 hours at room temperature, followed by 90 minutes at 65°C and another 90 minutes at 130°C. Samples were cured between two aluminum adherends. The adherend surface was grinded and cleaned with acetone prior to the application of the resin and the bondline thickness was controlled as 100 μm with silicon glass fiber. Teflon sheets were obtained from Fluoro-Plastics Co., with a thickness of 127um.

Equipment: Dielectric relaxation spectra were collected with a Novocontrol α Analyzer (3 μHz – 10 MHz).

Results and Discussion

Figure 4.1.1.3 shows the comparison of DRS results from "perfect" and "imperfect" joints, with the sample description in Table 4.1.1.1. In samples 30, 32 and 33, one or two Teflon patches were placed in the middle of the samples, schematically shown in Figure 4.1.1.1(b). The Teflon patches have a twofold effect on the DRS measurements: 1) increase the bond thickness because the patches are thicker than the spacer; and 2) decrease the area of the adhesives in contact with the adherend. In our measurements, we always used the dimensions of "perfect" samples, therefore overestimating the area and underestimating the thickness of the joint.

Since

Equation 4.1.1.1
$$\varepsilon_r^* = \frac{Cs^*}{\varepsilon_0}\frac{d}{A}$$

where ε_r^* is the complex dielectric permittivity; Cs^* is the measured complex capacitance of the sample; d is the thickness of the sample; A is the area of the sample.

Both the overestimation of the area and the underestimation of the thickness decrease the measured value. This is in agreement with the results shown in Figure 4.1.1.3, where both the permittivity and loss in imperfect samples are lower than those in the "perfect" sample (Jnt 12).

DRS study shows that defects always decrease the DRS measurement results.

Figure 4.1.1.1 Schematic of joints with no defects (a) and with one Teflon patch in the middle (b). Black area is for the adherends, grey area for the adhesives, and white area for Teflon patches.
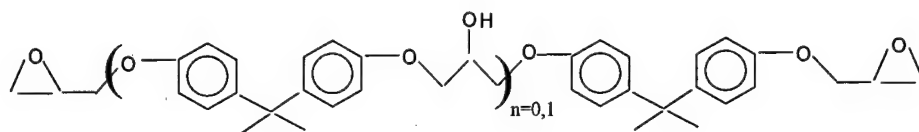
DGEBA
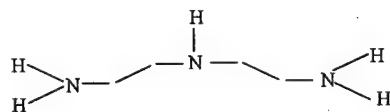
DETA

Figure 4.1.1.2 Chemical structures of diglycidyl ether of bisphenol A (DGEBA) and diethylene triamine (DETA).
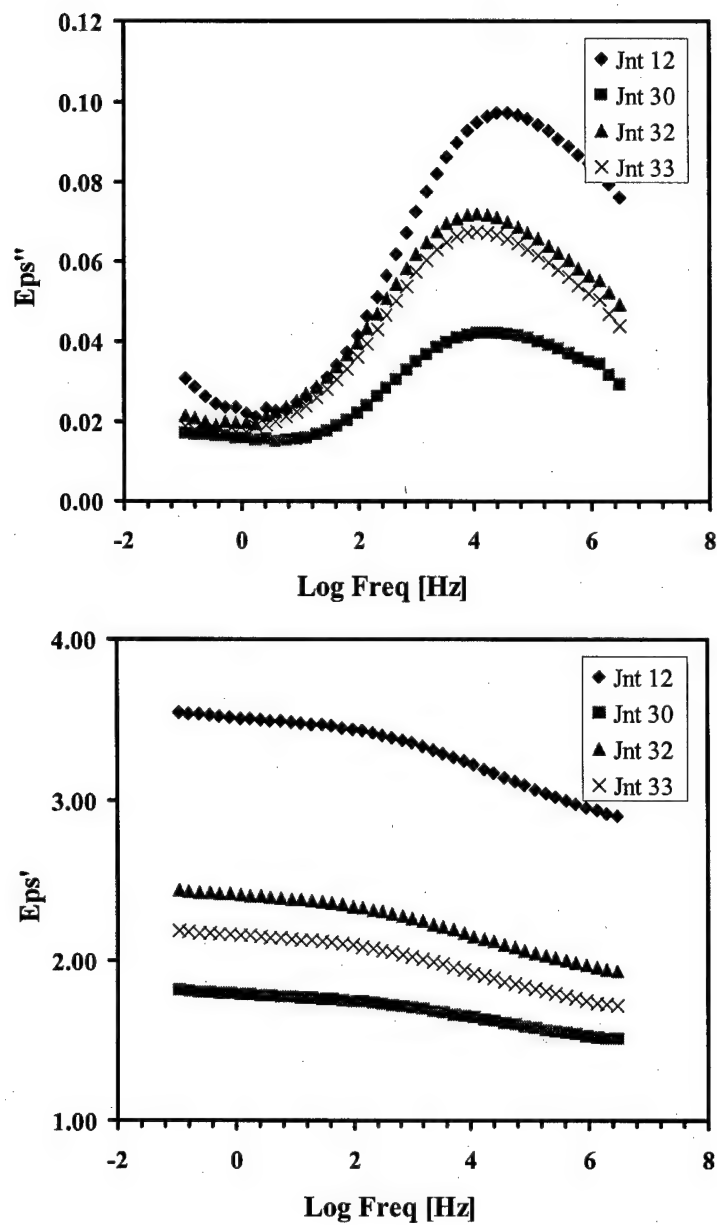
Figure 4.1.1.3   Comparison of DRS spectra of "perfect" and "imperfect" adhesive joints, with the description of the code listed in Table 4.1.1.1

Table 4.1.1.1 Description of joints in Figure 4.1.1.3

Joint No.	Description of defect
Jnt 12	No defect.
Jnt 30	A circular Teflon patch in the center of the joint.
Jnt 31	A half circle on the edge of the joint.
Jnt 32	A strip of Teflon placed across the middle of the joint.
Jnt 33	Two rectangular pieces of Teflon placed in the middle of the joint.

4.1.2 Time Domain Reflectometry (TDR)

Experimental

Materials: Due to the difficulty in making long strips with uniform thickness, we first studied the influence of defects with Teflon and water. To model possible defects, we left an air gap in the measurement strip, as shown in Figure 4.1.2.1.

Equipment: TDR test was run on network analyzer HP 8752A; the frequency range is 10^5 - 1.3×10^9Hz.

Results and Discussion

The effect of an air gap on the Teflon strip TDR traces is shown in Figure 4.1.2.2 with the blue solid and pink dashed curves for "perfect" and "imperfect" joints, respectively. The negative peak at time less than 0 ns is caused by the contact between the connector and the adhesive joint; we designate this point in time equal to 0. The first peak in the blue solid curves at positive time (t>0), with reflection coefficient of about 0.8, is from the end of the strip; we designated this point as 1. In the results for 390mm sample with air gap (pink dashed curve in Figure 4.1.2.2 (a)), we see a small peak between 0 and 1, which is due to the air gap. This peak could also be seen in the results for a 260 mm sample (Figure 4.1.2.2 (b)). In the results for the 145 mm strip (Figure 4.1.2.2 (c)), this small peak between 0 and 1 could not be seen.

This is because in the time domain measurement, the minimum distance between two responses in the reflection mode TDR may be calculated by:[3]

Equation 4.1.2.1   Min Distance = Impulse Width × (Speed of Light × velocity factor)

Where Impulse Width = 1.98 / highest frequency (s); Speed of Light = 3 × 10^{10}cm/s; and velocity factor = 1/ $\sqrt{\varepsilon_r}$, ε_r is the dielectric constant of the material.

With the above equation, the minimum distance between two responses with equal strength is calculated and listed in Table 4.1.2.1. Note that the increase of the highest frequency used and/or the dielectric constant of the material will enhance the resolution of the TDR tests. To prove that, we investigated the TDR traces of water strips with 0 -3 discontinuities (see Figure 4.1.2.3). We can see that for the 150 mm water strips, the three defects are easily discerned; the much higher resolution compared with adhesive structures is due to water's high dielectric permittivity.

In real adhesive application, especially aerospace industry, an adhesive joint with length longer than 390 mm (Figure 4.1.2.2 a) is quite common and thus the TDR test is appropriate for the detection of defects.

a   b

Figure 4.1.2.1 Schematic of the measurement strip with no defects (a), and with one defect in the middle (b).
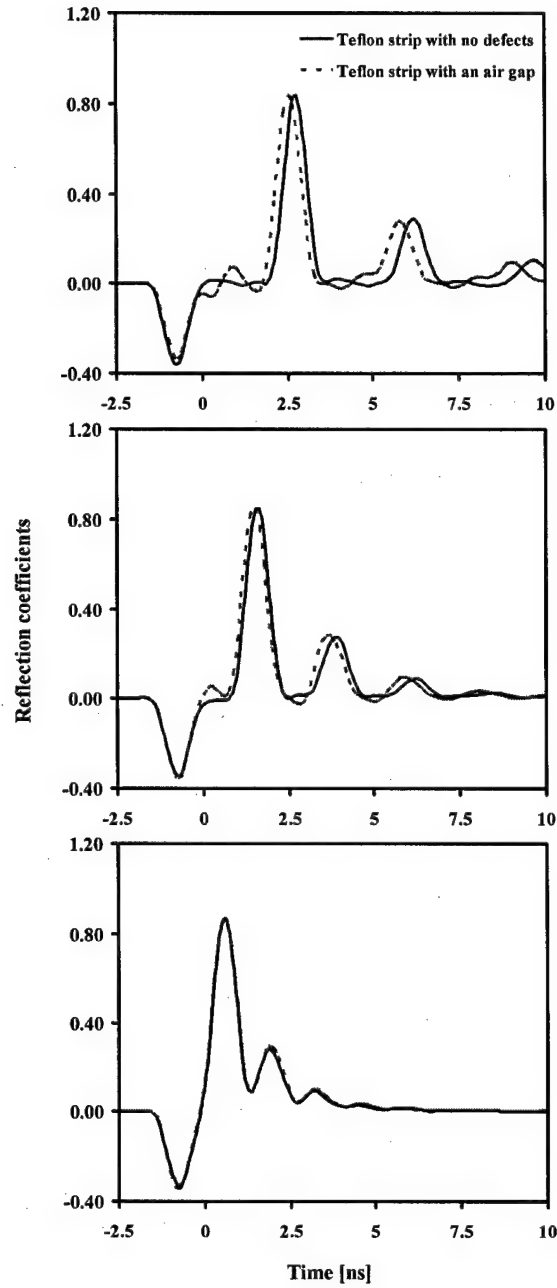
Figure 4.1.2.2 TDR results of Teflon strips of different lengths (390 mm (a), 260mm (b), and 145 mm (c)). Possible defects were modeled with a 30 mm air gap lying in middle of the strips. TDR traces without and with defects are shown with blue solid and pink dashed curves, respectively.

Table 4.1.2.1 Minimum distance between two TDR traces with equal strength (cm)

material	ε_r	highest frequency (GHz)			
		1.30	3.00	6.00	9.00
Teflon	2	7.83	3.39	1.70	1.13
Epoxy	4	5.54	2.40	1.20	0.80
Water	80	1.24	0.54	0.27	0.18
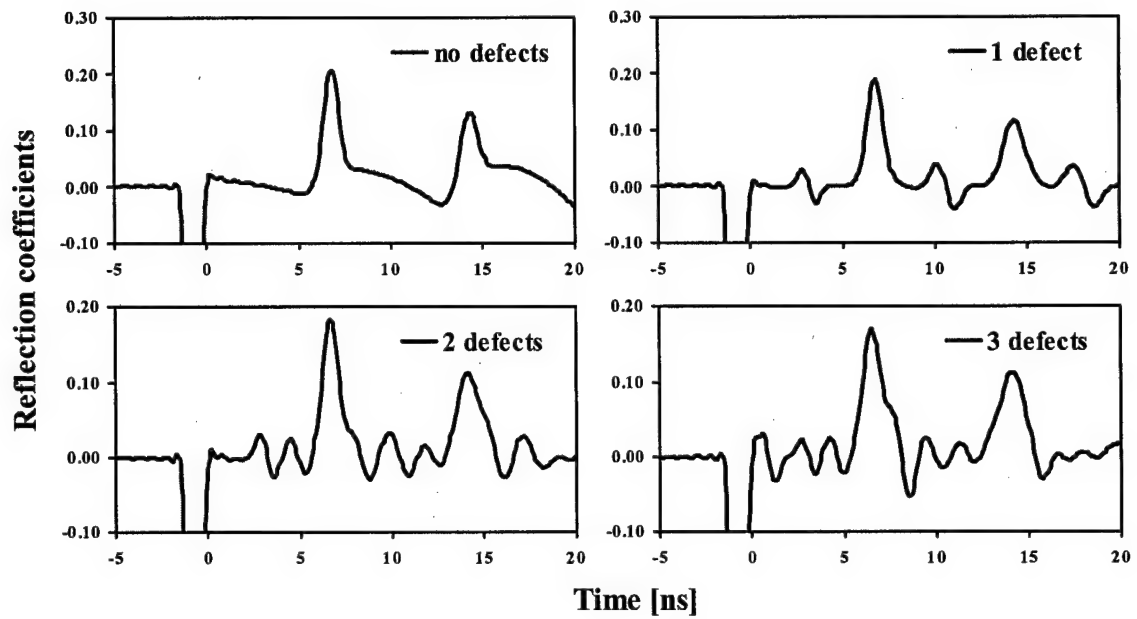
Figure 4.1.2.3 TDR responses of 150 mm water strip with 0, 1, 2, and 3 Teflon patches. The 1st, 2nd and 3rd patch were put at ½, ¾, and ¼ of the water strip length from the connector.

4.2   Effect of Water Exposure

We studied the effects of water exposure on adhesive joints using four techniques: DRS (including two-dimensional DRS), TDR, fiber-optic Near Infrared and molecular dynamics simulation.

4.2.1   DRS

This part of our study was conducted in three stages: first, the molecular origin of relaxation processes of epoxy amine adhesive network was examined; then, based on that knowledge, the effect of moisture on adhesive joints in the initial (pre-damage) stage of absorption was investigated. And finally, the effect of long time water exposure on adhesive joints was studied.

Experimental

Materials: Two model epoxy-amine formulations and one commercial adhesive system were used. The two model systems are DGEBA-DETA and DGEBA-TEPA (tetraethylene pentamine, chemical formula shown in Figure 4.2.1.1). DGEBA, DETA and TEPA were obtained from Aldrich Chemical Company and were used as received. The curing procedure is same as described in section 4.1.1.

The commercial system we used is Epibond 1590, from Vantico Inc. Epibond 1590 is believed to have the following components:

Component A (Resin)

- 30% is N,N,N',N'-tetraglycidyl-4,4'-diaminodiphenylmethane (Figure 4.2.1.2 a)

- 40% is epoxy phenol novolak resin (Figure 4.2.1.2 b)

- 30% is triglycidyl-p-aminophenol (Figure 4.2.1.2 c)

Component B (Hardener)

- 20% is tetraethylene pentamine (Figure 4.2.1.1)

- 15% is 2-piperazine-1-ethylamine (Figure 4.2.1.2 d)

- 15% is cycloaliphatic polyamine

The cure cycle consists of three stages: 4 hours at 40°C, followed by 1 hour at 80°C, and 2 hours at 150°C.

Aging and Testing Conditions: For short exposure study, samples were kept at 80°C/98% Relative Humidity (RH) for selected time, weighed and tested. For long time exposure, samples were aged under two conditions: (1) immersion in 65°C water and (2) immersion in 100°C boiling water for selected time, followed by gravimetric and dielectric analysis.

Equipment: Broadband dielectric relaxation spectra were collected on a Novocontrol α Analyzer (3 μHz – 10 MHz) and a Hewlett-Packard 4291B RF Impedance Analyzer (1 MHz - 1.8 GHz). Sample weight was recorded on a Mettler Toledo AX105 balance, with a precision range of +/- 0.005mg. Supporting evidence was obtained from Fourier transform infrared (FTIR) spectroscopy, using Nicolet Instrument's Magna 750 Spectrometer, and differential scanning calorimetry (DSC), using Perkin-Elmer model 7 DSC at a heating rate of 10°C/min. Molecular simulation was run with a commercial software Materials Studio (Accelrys, Inc.).
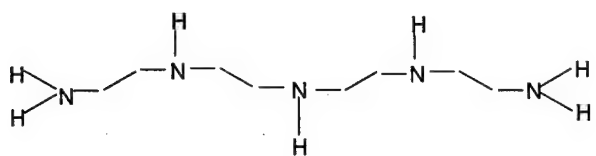
Figure 4.2.1.1 Chemical structure of tetraethylene pentamine (TEPA).

N,N,N',N'-tetraglycidyl-4,4'-diaminodiphenylmethane **a**

epoxy phenol novolac resin **b**

triglycidyl-p-aminophenol **c**
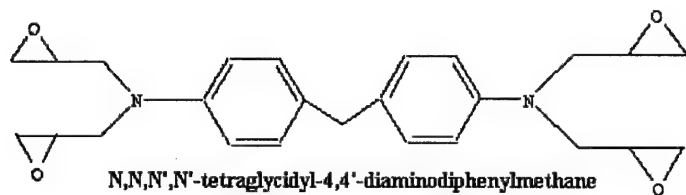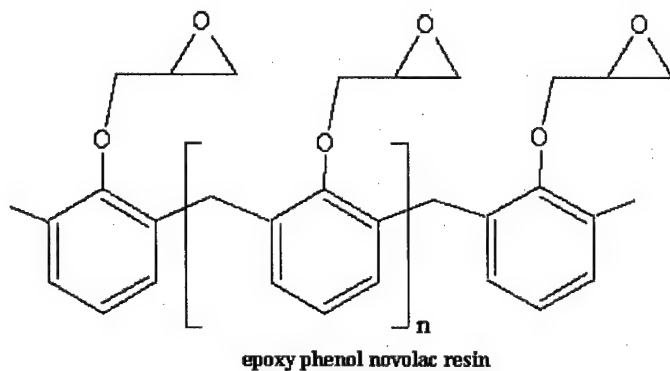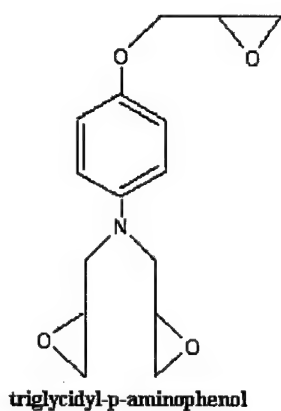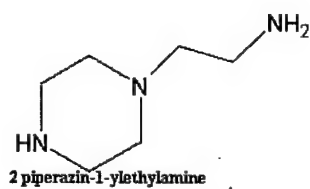
2 piperazin-1-ylethylamine **d**

Figure 4.2.1.2 Constituents of the Epibond 1590 adhesive components A (a, b, c) and B (d).

4.2.1.1 Dry Systems

4.2.1.1.1 Model System I ---- DGEBA-DETA system[1]

In Figure 4.2.1.3 we show dielectric loss in the frequency domain at various temperatures below 60°C. Two local relaxation processes are observed and termed β and γ in the order of increasing frequency at a constant temperature; a deconvoluted spectrum at -60°C is shown in the inset, with solid lines representing the Cole-Cole functional form. Both β and γ processes have Arrhenius temperature dependence with activation energy of 60 and 40 kJ/mol, respectively.

Figure 4.2.1.3 Dielectric loss in the frequency domain of dry stoichiometric DGEBA-DETA polymer network with the measuring temperature as a parameter. The inset shows a deconvoluted dielectric loss spectrum measured at -60°C (213K).

A prerequisite for the study of chemo-physical interactions between the network and the absorbed moisture is an understanding of the molecular origin of β and γ relaxations in the dry network. Earlier studies suggested that β and γ relaxations in epoxy networks were related to the localized motions of hydroxyl groups and ether linkage of the glycidyl moiety, respectively. In order to verify this, we have undertaken a systematic investigation of a series of dry, cured, off-stoichiometric DGEBA-DETA formulations. By varying the stoichiometry we were altering, in a quantitatively controlled manner, the relative ratios of four dipolar moieties (hydroxyl, ether, amine and epoxy) in the network and observing the ensuing effect on the DRS spectra. In the discussion that follows, all formulations are defined by the epoxy (E) to amine hydrogen (A) ratio normalized with respect to one epoxy group; for example, the 1E:1A ratio denotes a stoichiometric mixture. Subscripts E and A are used in the off-stoichiometric mixtures to distinguish between the relaxation processes in epoxy rich (β_E and γ_E) and amine rich (β_A and γ_A) formulations. No subscripts are used for relaxations in the dry stoichiometric formulation. The results obtained on the off-stoichiometric formulations proved quite revealing, as we consider the epoxy rich formulations first.

A typical example of dielectric loss in the frequency domain for several epoxy rich formulations and neat DGEBA measured at $-60^{\circ}C$ is given in Figure 4.2.1.4. Measurements conducted at various temperatures between $-80^{\circ}C$ and $+60^{\circ}C$ yielded analogous results and are not shown here. The intensity and the dielectric relaxation strength, $\Delta\varepsilon_{\beta E}$, defined as $\Delta\varepsilon_{\beta E} = \varepsilon_0 - \varepsilon_\infty$ of the β_E process (seen at lower frequency in Figure 4.2.1.4) decrease with an increase in the E:A ratio. This finding is readily rationalized: hydroxyl groups, that are at the heart of the β process, are the product of

21

epoxy-amine reactions and their concentration decreases with an increase in the E:A ratio. A slight increase in the average relaxation time (shift to lower frequency) of the β_E process with increasing E:A ratio is attributed to the difference in the local environment (different chemical composition as a result of different epoxy/hydroxyl ratio, different crosslinking density, different departure from Tg, etc). As a point of information we note that the calorimetric Tg (which reflects segmental, not local motions), increases from -12°C, to 31°C, to 48°C, to 120°C with a decrease in the E:A ratio from neat DGEBA, to 1:0.33, to 1:0.5, to 1:1.

The intensity and the dielectric relaxation strength of the γ_E process (seen at higher frequency in Figure 4.2.1.4) increase with increasing E:A ratio. Similar process is also seen in the neat DGEBA and hence the γ_E process was assigned to the relaxation of the remaining (unreacted) glycidyl groups. Especially interesting is the presence, at all temperatures, of an isosbestic point in the DRS spectra, i.e. frequency at which the dielectric loss is independent of the composition. The presence of an isosbestic point is a signature of two relaxation processes. We also observe a shift in the isosbestic point to higher frequency by approximately one decade for every 20°C.
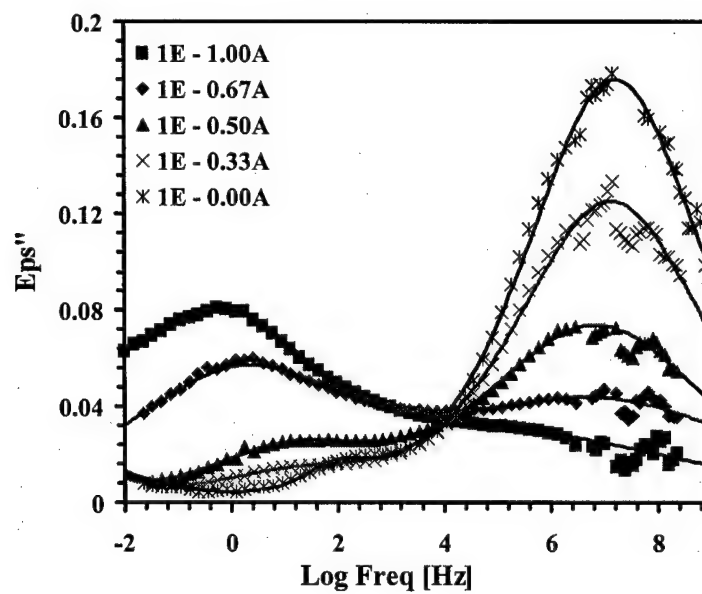
Figure 4.2.1.4 Dielectric loss in the frequency domain for a series of epoxy-rich DGEBA-DETA networks and neat DGEBA measured at –60°C.

We now briefly examine amine rich formulations. The relaxation spectra of networks with E:A ratios ranging from 1:1 to 1:5 were fit with two Cole-Cole (CC) equations and the relaxation strength of the β_A and γ_A processes ($\Delta\varepsilon_{\beta A}$ and $\Delta\varepsilon_{\gamma A}$, respectively) was calculated. Figure 4.2.1.5 includes the relaxation strength of β and γ processes in amine- and epoxy-rich networks. We observe that $\Delta\varepsilon_\beta$ increases with increasing amount of amine when E:A$\geq$1, because of the concomitant increase in the concentration of hydroxyl groups. A further increase in the amine concentration beyond the stoichiometric ratio (i.e., when E:A>1) has no effect on $\Delta\varepsilon_\beta$.

A composite plot of frequency at maximum loss (Freq$_{max}$) as a function of reciprocal temperature for networks with different E:A ratios is shown in Figure 4.2.1.6. An Arrhenius temperature dependence was observed and the calculated activation energy for the β and γ process of 60 and 40 kJ/mole, respectively, was independent of the E:A ratio.

In sum, it is safe to say that the DRS spectra of dry networks with varying stoichiometry provide further evidence that the β process is associated with hydroxyl groups while the γ process involves primary and secondary amine and ether groups.
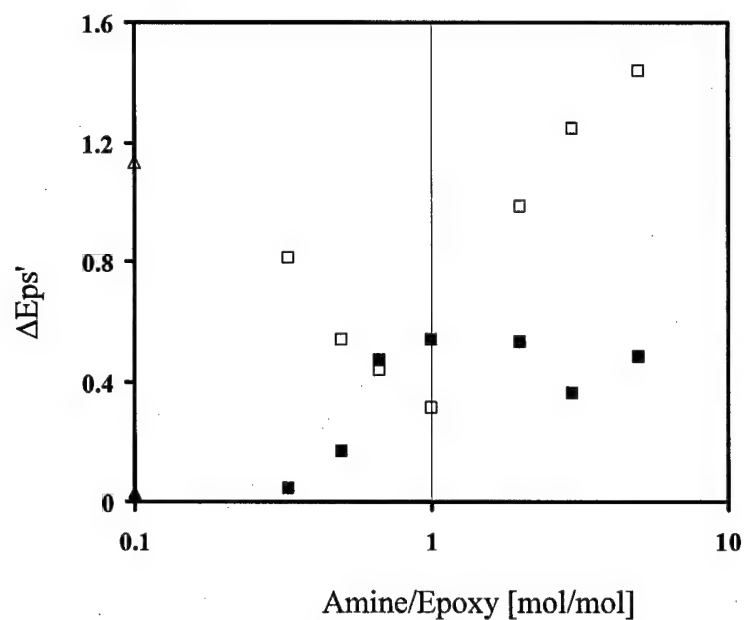
Figure 4.2.1.5 Dielectric relaxation strength of β and γ processes at different E:A ratios. Solid and open squares describe the β and the γ process of networks, respectively. Triangles (on the ordinate) describe β and γ processes in the neat DGEBA.
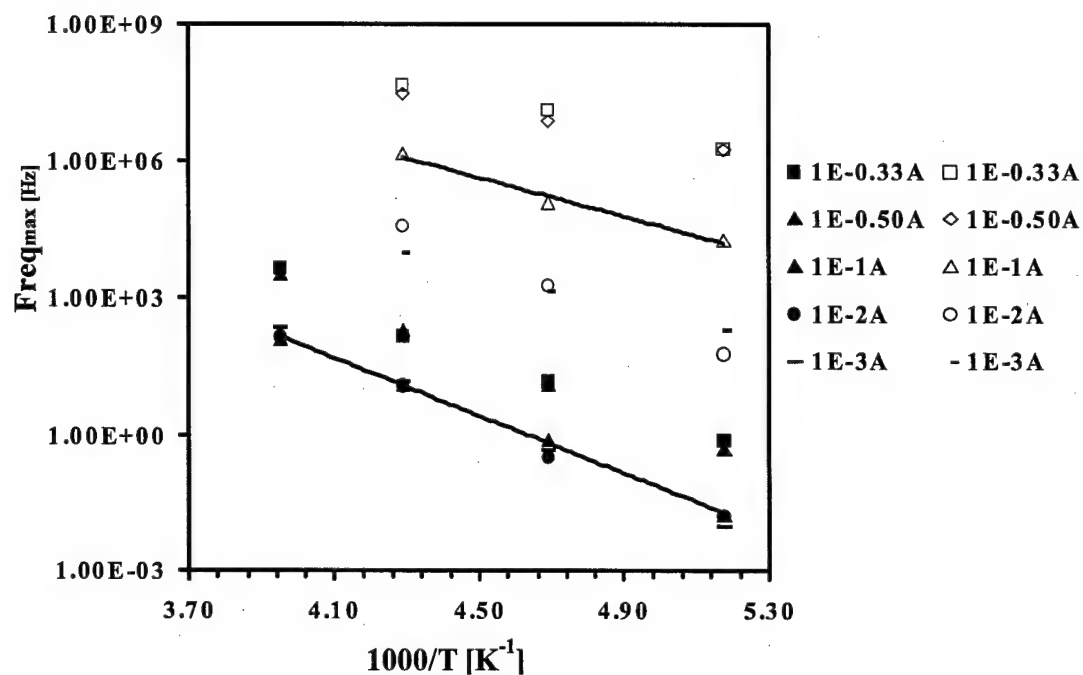
Figure 4.2.1.6   Frequency at maximum loss as a function of reciprocal temperature for a series of stoichiometric and off-stoichiometric networks. Solid and open symbols describe the β and the γ process, respectively.

26

4.2.1.1.2 Model System II ---- DGEBA-TEPA system

During the 2002 annual review meeting of the Polymer Matrix Composite Program in Long Beach, it was suggested that DETA could diffuse to the surface of adherends during cure leading to its non-uniform distribution and hence non-uniform mechanical properties of the joints. But another multifunctional amine, tetra-ethylene-pentamine (TEPA), was believed to show no preference toward surface migration and hence lead to a uniform cure. That prompted us to test TEPA as curing agent and check the results against those obtained for the DGEBA-DETA system. The effect of water absorption on the DGEBA-TEPA system was also studied for short exposure times.

Shown in Figure 4.2.1.7 are spectra of dry samples. We can see a clear sub-Tg relaxation; its shape and position are practically identical to those of the DGEBA-DETA system. Similarly to the DGEBA-DETA system, the DRS spectra of dry DGEBA-TEPA networks could also be deconvoluted into two sub-Tg processes at temperature lower than -30°C (243K). Later (in section 4.2.1.1.4), we will compare those relaxation times with DGEBA-DETA and Epibond 1590 systems.

4.2.1.1.3 Commercial System ---- Epibond 1590 system

Epibond 1590 is a commercial adhesive for bonding carbon fiber reinforced plastic and aluminum components for aircraft structures. It is said to have an excellent balance of toughness and high temperature performance, as well as excellent resistance to environmental attack. The possible structures of the two components are described in the experimental part. The DRS spectra of dry Epibond 1590 are shown in Figure 4.2.1.8.

Similarly to the above described model systems, the dry spectra of Epibond 1590 below -30°C (243K) could also be deconvoluted into two sub-Tg peaks.

4.2.1.1.4 Comparison of DRS spectra between DGEBA-DETA, DGEBA-TEPA, and Epibond 1590 systems

Figure 4.2.1.9 shows the relaxation frequencies of the two sub-Tg processes in DGEBA-DETA, DGEBA-TEPA and Epibond 1590 systems as a function of reciprocal temperature. We could see that in those systems, the relaxation times of β and γ are practically identical, probably because of their common molecular origin.
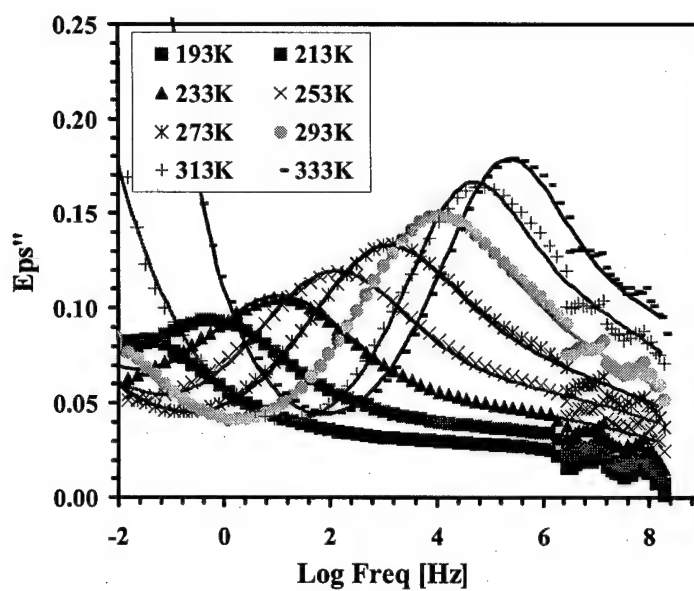
Figure 4.2.1.7 Dielectric loss in the frequency domain of dry stoichiometric DGEBA-TEPA polymer network with the measuring temperature as a parameter.
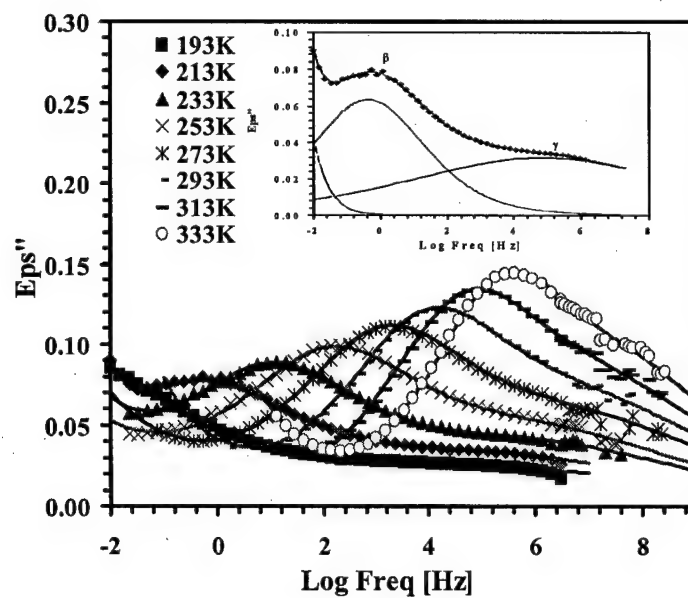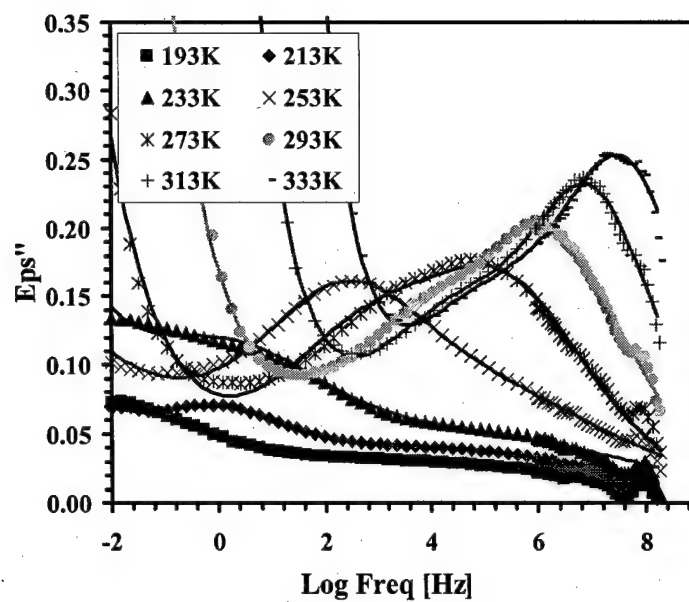
Figure 4.2.1.8   Dielectric loss in the frequency domain of dry stoichiometric Epibond 1590 polymer network with the measuring temperature as a parameter.
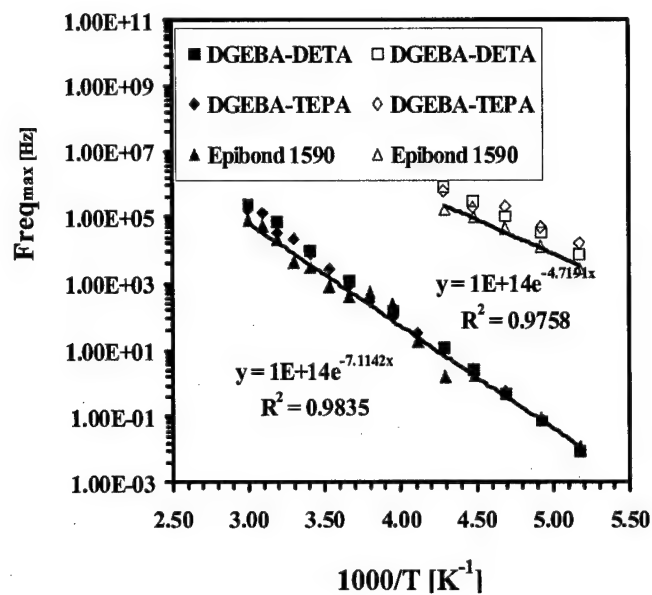
Figure 4.2.1.9 Frequency at maximum loss as a function of reciprocal temperature for DGEBA-DETA, DGEBA-TEPA and Epibond 1590 system. Solid and open symbols describe the β and the γ process, respectively.

4.2.1.2   Short Time Exposure

4.2.1.2.1 Model System I ---- DGEBA-DETA system

We now consider how the acquired understanding of the molecular origin of local relaxations can help us elucidate the interactions between the polymer network and the absorbed moisture. In the process of doing so we shall examine the DRS spectra of samples of different stoichiometry, at different levels of moisture uptake and at different measuring temperatures. The variation in stoichiometry has a profound effect on the dielectric response of moist samples, as illustrated below. The results for the epoxy rich formulations are exemplified in Figure 4.2.1.10, which shows dielectric loss in the frequency domain for a 1E:0.5A formulation measured at $-80°C$, with moisture content (%) as a variable. Note a systematic increase in the relaxation strength of the β_E process and a simultaneous decrease in the strength of the γ_E process. Both changes are irreversible, as clearly established by examining the spectrum of a redried sample. An explanation was sought and obtained with the aid of near-FTIR (NIR) and mid-FTIR (MIR) measurements, briefly described below. The characteristic NIR and MIR absorption bands in epoxy-amine formulations are well-documented and we shall omit reviewing them here. In Figure 4.2.1.11, we show a series of NIR spectra of a 1E:0.5A network taken at various times during moisture uptake. Note the increase in the intensity of the characteristic peaks due to absorbed water (at 5235 cm^{-1}) and hydroxyl groups (at 7000 cm^{-1}). Surprisingly, however, there is a simultaneous decrease in the intensity of epoxy absorption (at 4530 and 6000 cm^{-1}). That observation, taken together with the irreversible increase in the hydroxyl absorption band at 7000 cm^{-1} (analogous

observations were made in the MIR spectra not shown here), leaves little doubt that a chemical reaction occurs between epoxy groups and water. This was intuitively unexpected and a number of model systems were examined to provide corroborating evidence. We shall not be comprehensive here; suffice it to say that the epoxy-water reaction will take place in the presence of a tertiary amine catalyst. For example, NIR spectra of neat DGEBA in contact with water vapor at 80°C did not change at all with exposure time in excess of 24 hours, while a dramatic change (increase in hydroxyl absorption, decrease in epoxy absorption) was observed upon the addition of a small amount of tertiary amine that acts as a catalyst for the reaction between DGEBA and water. The possibility of chemical reaction between epoxy group and water is of further practical importance in the light of the frequent use of epoxy rich formulations as matrices in composite materials.

Reverting our attention to the dynamics of the β_E process in moist samples, we observed a gradual increase in the average relaxation time (see Figure 4.2.1.10) followed by leveling off at about 1.5% water content. A further increase in the average relaxation time for the β_E process was noted in the redried samples. Analogous trends were observed at different measuring temperatures.

The intensity and the relaxation strength of the γ_E process decrease with moisture uptake. Considering that the γ_E process comprises local relaxations of epoxy rings, the observed decrease in $\Delta\varepsilon_{\gamma E}$ is in agreement with the depletion of epoxy groups due to chemical reaction during moisture uptake.
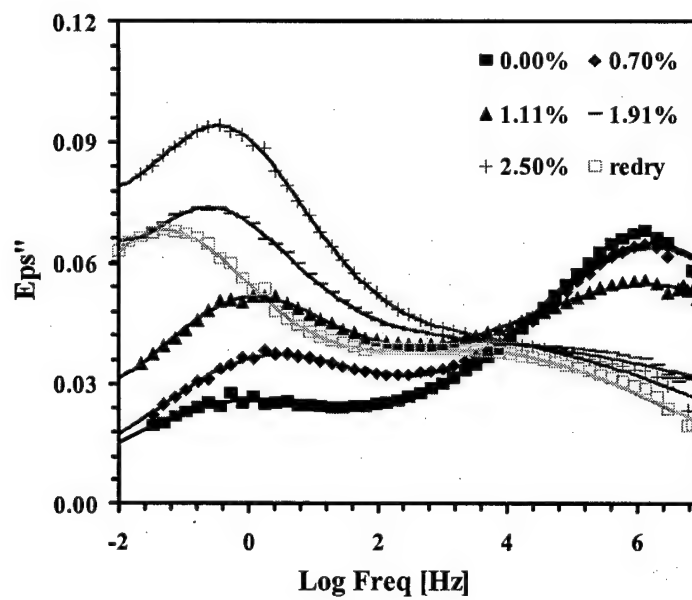
Figure 4.2.1.10 Dielectric loss in the frequency domain for a 1E:0.5A DGEBA-DETA network with moisture content as a parameter, measured at -80°C.
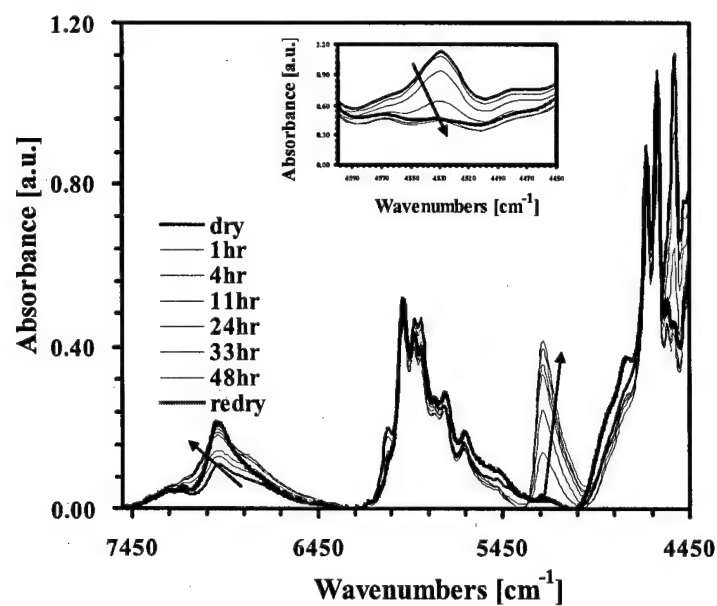
Figure 4.2.1.11 NIR spectra at different exposure times of a 1E:0.5A network. In the direction of the arrow, the spectra correspond to dry, 1hr, 4hr, 11hr, 24hr, 33hr, and 48hr. The two thicker curves are for dry (bottom) and for redried (middle) sample; the increase of hydroxyl groups in the 6200-7450 cm^{-1} and consumption of epoxy groups in the 4800-4400 cm^{-1} range are clearly seen in the inset.

The effect of moisture on the dynamics of the amine rich formulations is also evident in the range of β_A relaxation (Figure 4.2.1.12) and is attributed to the interaction between hydroxyl groups and water molecules during moisture uptake. Two interesting observations were made that stand in contrast with the epoxy rich formulations: 1) the average relaxation time for the β_A process decreases (shifts to higher frequency) with increasing moisture content, and 2) the observed increase in the intensity and the dielectric relaxation strength that accompany moisture uptake are fully reversible. This is illustrated in the dielectric spectrum of Figure 4.2.1.12 for a 1E:2A formulation measured at -60°C, with moisture content (%) as a parameter. Analogous DRS results were obtained at other measuring temperatures and no changes were observed in the NIR and/or MIR spectra of dry and redried samples. The effect of absorbed moisture on the γ_A process is negligible. A possible explanation could be sought in the water-amine interactions that result in the formation of a quaternary ammonium cation and a hydroxyl anion that contribute to conductivity rather than relaxation. Some support for this hypothesis comes from the higher values of the measured conductivity and diffusion coefficient in the amine rich networks.
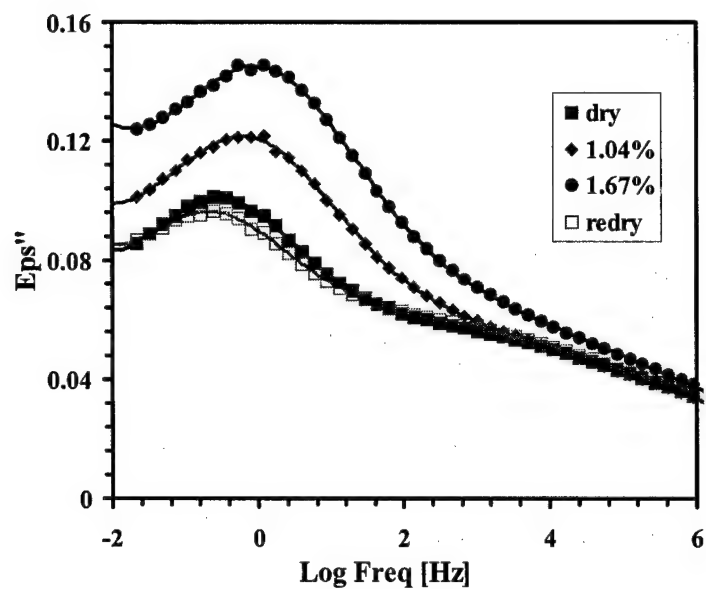
Figure 4.2.1.12 Dielectric loss in the frequency domain for 1E:2A DGEBA-DETA network with moisture content as a parameter, measured at –60$^{\text{O}}$C.

We now return our attention to the stoichiometric formulation and examine in further detail the effect of absorbed moisture on the local dynamics and the molecular origin of water-network interactions. We preface the presentation and discussion of these results with two comments. First, we stress that we shall not be principally concerned with the kinetics of moisture absorption. We limit ourselves to saying that the diffusion process is Fickian and that the calculated value of the diffusion coefficient of $4.42*10^{-8}$ $cm^2 s^{-1}$ is in agreement with the literature. And second, we acknowledge efforts to monitor moisture absorption in polymers by tracking dielectric permittivity at a constant frequency but hasten to add that our DRS spectra were recorded and quantified over a wide frequency range. In Figure 4.2.1.13 we show dielectric loss in the frequency domain with moisture content (%) as a parameter measured at $-60^{\circ}C$. Again, analogous results were obtained at other measuring temperatures and are not shown here. The intensities of β and γ processes increase with moisture uptake, and the moisture absorption is fully reversible, as shown in the redried spectrum in Figure 4.2.1.13. Interestingly, the average relaxation time for the β process decreases with moisture uptake.
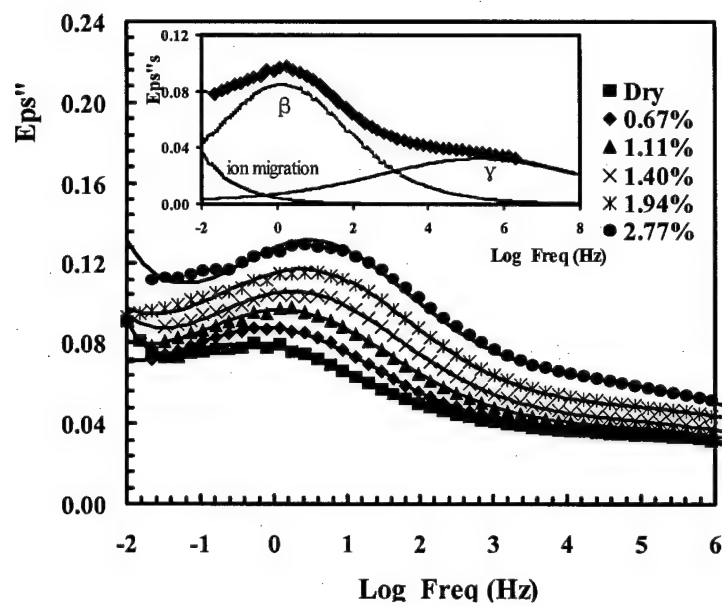
Figure 4.2.1.13 Dielectric loss in the frequency domain for 1E:1A DGEBA-DETA network with moisture content as a parameter, measured at –60°C.

To quantify the net effect of the absorbed water on the local dynamics, spectral subtraction was performed and the resulting difference spectra are shown in Figure 4.2.1.14. The two processes (β_m and γ_m) can be readily deconvoluted and fitted with two Cole-Cole functions at temperatures below $-30^{\circ}C$ (shown in the inset of Figure 4.2.1.14). Subscript m is used in the text below to distinguish moist from dry (no subscript) stoichiometric networks. The following equation was used to fit the data:

Equation 4.2.1.1
$$\Delta\varepsilon^* = \frac{\Delta\varepsilon_{\beta m}}{1+(i\omega\tau_{\beta m})^{a_{\beta m}}} + \frac{\Delta\varepsilon_{\gamma m}}{1+(i\omega\tau_{\gamma m})^{a_{\gamma m}}} + \Delta\varepsilon_U$$

In Equation 4.2.1.1, $\Delta\varepsilon$ is the relaxation strength, τ the relaxation time, a the Cole-Cole parameter, the subscripts βm and γm refer to the β and γ processes in the difference spectra of moist networks, and ε_U is the limiting high-frequency permittivity. Above $-30^{\circ}C$, however, deconvolution is too uncertain to be considered physically meaningful. Both β_m and γ_m relaxations have an Arrhenius temperature dependence (Figure 4.2.1.15) with an activation energy of ca. 58kJ/mol.
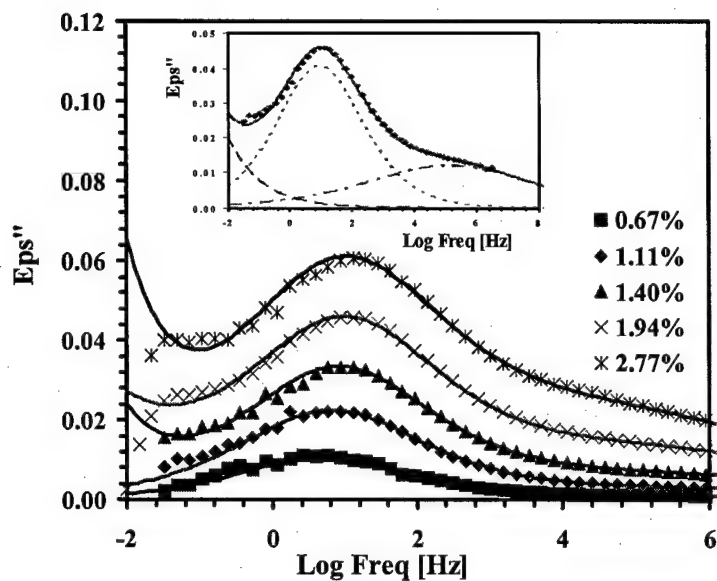
Figure 4.2.1.14 Difference dielectric spectra of 1E:1A DGEBA-DETA network in the frequency domain with moisture content as a parameter, measured at -60°C. The inset shows a deconvoluted difference spectrum of 1E:1A DGEBA-DETA network with the aid of two Cole-Cole functions and a low-frequency dc conductivity dependence (with 1.94% moisture, measured at -60°C).
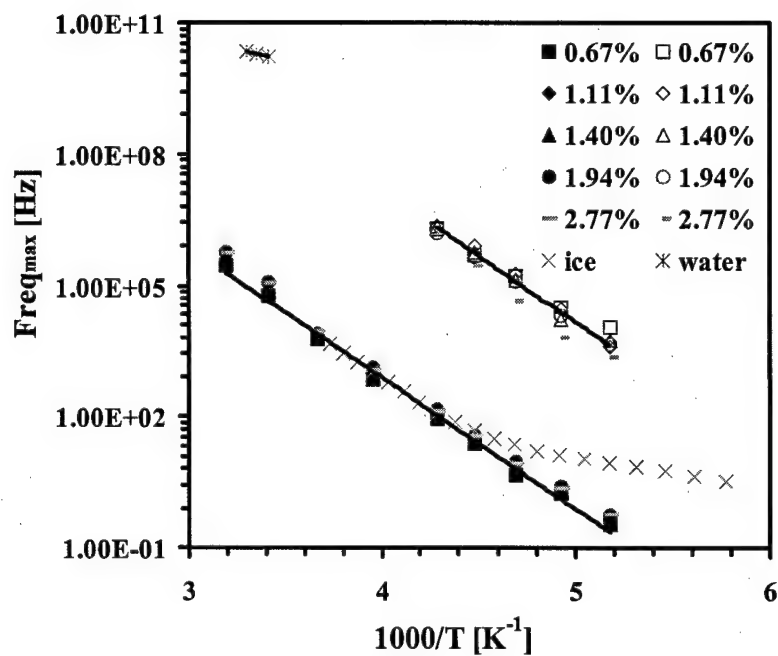
Figure 4.2.1.15 Frequency at maximum loss as a function of reciprocal temperature for β_m (solid symbols) and γ_m (open symbols) relaxations, with moisture content as a parameter. Also shown are the frequency at maximum loss data for ice (X) and liquid water (*).

At this point, notwithstanding the form in which water resides in the network, it is instructive to compare our results with the dynamics of (isotropically mobile) bulk liquid water and ice. For that purpose we have included in Figure 4.2.1.15 data for pure liquid water and ice. At 20°C liquid water has a dielectric loss peak at about 20 GHz, corresponding to an average relaxation time of ca. 9ps. This is faster than the extrapolated value for the γ_m process and many orders of magnitude faster than the β_m process. Dielectric spectra of pure ice are also very interesting; the average relaxation time for ice is commensurate with that for the β_m process between 0 and -40°C but becomes faster below that temperature. We report the coincidence of the data for ice and moist network in the 0 to -40°C range as a curiosity and no further attempts were made at clarifying the molecular origin of that observation. Because bulk liquid water relaxes at much higher frequency (and water vapor at still higher frequency) than the β_m or the γ_m process, the contribution (if any) from liquid water or vapor to the dielectric permittivity of moist networks ought to be contained within the $\Delta\varepsilon_U$ term. Of course, that term contains the contribution from atomic and electronic polarization from all water molecules and hence an increase in $\Delta\varepsilon_U$ with moisture would suggest an increase in the content of the isotropically mobile water (or vapor). Furthermore, since the β_m process originates from the interactions between water and hydroxyl groups and the γ_m process in the interactions between water and glycidyl ether groups, the relative change in the strength of these two relaxations with moisture content should provide a clue about the ratio of water hydrogen-bonded to hydroxyl and to glycidyl ether groups. Changes in the dielectric relaxation strength of β_m and γ_m processes and the $\Delta\varepsilon_U$ term were calculated as a function of moisture content and plotted in Figure 4.2.1.16. It is immediately clear that the

increase in the relaxation strength of the β_m ($\Delta\varepsilon_{\beta m}$) and/or the γ_m ($\Delta\varepsilon_{\gamma m}$) process is much greater than the increase in $\Delta\varepsilon_U$ indicating a strong preference of the absorbed moisture for participation in the β_m and γ_m processes. Dashed line shown in Figure 4.2.1.16 is calculated from the following equation based upon the contribution from atomic and electronic polarization of total moisture:

Equation 4.2.1.2 $\Delta\varepsilon_U$ (atomic, electronic polarization) = [ε_∞(ice) - ε_∞ (dry resin)]×moisture content

The value of ε_∞ = 3.1 for ice was used in the calculation. As seen in Figure 4.2.1.16, the measured value of $\Delta\varepsilon_U$ is only slightly higher than the value calculated based on the contribution from atomic and electronic polarization; the difference between the two values of $\Delta\varepsilon_U$ amounts to about 5% of the total increase in the overall dielectric relaxation strength ($\Delta\varepsilon_{\beta m}$ + $\Delta\varepsilon_{\gamma m}$ + $\Delta\varepsilon_U$) due to moisture absorption. This suggests that, within the accuracy of the estimate and the measurement, the contribution of liquid (and/or vapor) water to $\Delta\varepsilon_U$ is on the order of 5%, implying that the majority of absorbed water relaxes as a part of the β_m and/or the γ_m process. The finding that only about 5% of the absorbed moisture in the DGEBA-DETA network is in the form of "free water" is in contrast with the earlier reports for bismaleimide (BMI) networks and other epoxy-amine networks. In BMIs, however, there is a likelihood of void formation as a result of etherification reaction and the absorbed water can accumulate in those voids. In the other epoxy-amine networks studied, the calculation of "free water" was based on the value of dielectric permittivity at 1MHz at room temperature; consequently, only the β process was considered as representative of "bound water", while the interactions that underlie the γ process were lumped under "free water", yielding the high reported value.

We acknowledge here the possibility that the change of free volume fluctuations and physical aging may affect the relaxation strength of the β process ($\Delta\varepsilon_\beta$). However, the change of free volume fluctuations induced by additives was reported to decrease $\Delta\varepsilon_\beta$ in some polymeric systems and to have no effect in others. Physical aging, on the other hand, is generally known to (slightly) decrease the relaxation strength of a sub-Tg relaxation. In our case, following a 60 day exposure to dry environment at 20°C, we measured a decrease in $\Delta\varepsilon_\beta$ of about 10^{-3}; a negligible change on the scale of Figure 4.2.1.14.
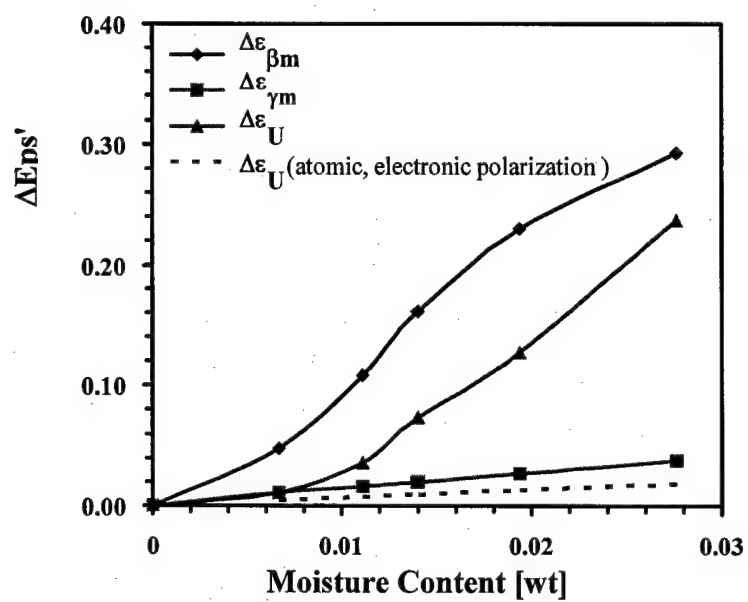
Figure 4.2.1.16 Dielectric relaxation strength of β_m and γ_m processes and the $\Delta\varepsilon_U$ term as a function of moisture content, measured at -60°C.

Although it is clear that moisture affects the local dynamics and that some details about the molecular origin of local relaxations can be gleaned from DRS, a great deal more can be learned about the nature of the network-water interactions from the FTIR spectra. Important unanswered questions are: 1) in what form (single molecules, dimmers, trimers, clusters) water resides within the adhesive; 2) at what network sites water forms hydrogen bonds; and 3) in how many hydrogen bonds a water molecules participates? To facilitate visualization and interpretation of the relevant molecular-level events we show in Figure 4.2.1.17 a schematic of a fragment of the network with absorbed water molecules. Possible network-water interactions are indicated by dashed lines.

A series of NIR spectra were taken at select time intervals during exposure to the environment. Difference spectra were then obtained by subtracting the spectrum of a dry network from that of each wet network and are displayed in Figure 4.2.1.18. Water uptake causes pronounced changes in the 4950-5400 cm^{-1} and 6200-7500 cm^{-1} range. The increase in the intensity of absorption in the 4950-5400 cm^{-1} range has been associated with the combination of asymmetric stretching (v_3) and bending deformation (v_2). Since hydrogen bonding has the opposite effect on stretching and bending vibrations, it is difficult to provide a molecular interpretation of the effect of moisture on the combination mode and no further attempts were made along those lines. Instead, attempts were made to quantify the absorption range of 6200-7500 cm^{-1}, which is attributed to hydroxyl vibrations. Deconvolution of the difference spectra reveals the presence of three absorption bands in that range, centered at 7085, 6834 and 6541 cm^{-1}, respectively. As an example we show in the inset of Figure 4.2.1.18, a deconvoluted difference spectrum for

a sample containing 0.46% moisture. Similar spectra were recorded for other systems that range from the liquid mixtures of water with polar and non-polar solvents to cross-linked thermoset networks.
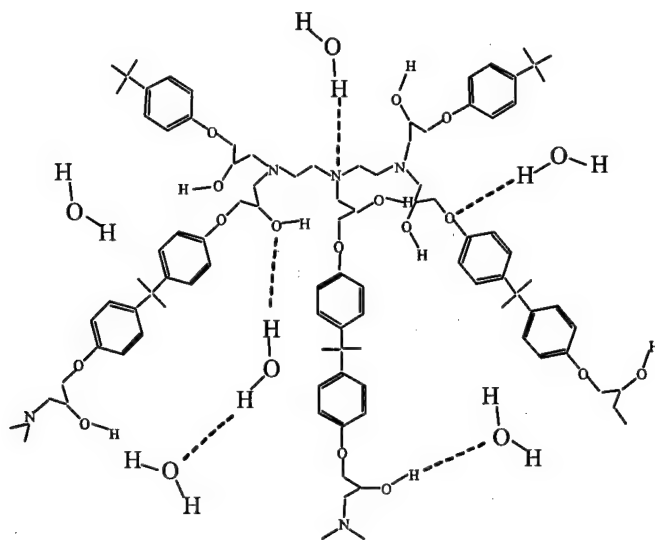
Figure 4.2.1.17 Schematic of a network fragment with absorbed water molecules; possible water-network interactions are indicated by dashed lines.
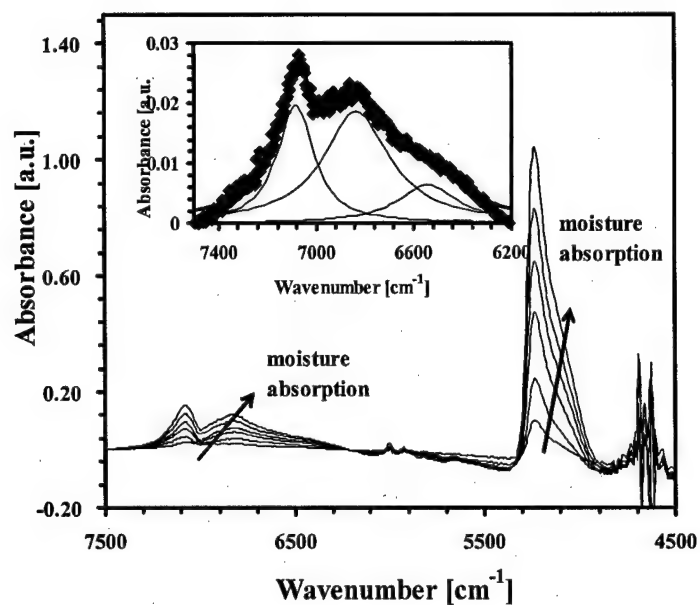
Figure 4.2.1.18 NIR difference spectra of 1E:1A DGEBA-DETA network with different moisture content. In the direction of the arrow, the moisture content (w/w) is: 0.46%, 1.02%, 1.58%, 2.03%, 2.41%, 2.69%. The inset shows a deconvoluted difference spectrum (7500-6200cm^{-1}) of a 1E:1A DGEBA-DETA network with 0.46% moisture content.

The key question regards the interactions that underlie those three deconvoluted peaks and an explanation is offered by postulating the existence of three spectroscopically distinguishable forms of hydrogen bonding, termed S_0, S_1 and S_2, where subscripts zero, one and two denote the number of hydrogen atoms of a water molecule that participate in hydrogen bonding. We note that hydrogen bonding via water oxygen is possible but is not recorded by this method. Based on the changes in the breadth and the full width at half height (fwhh) of the peaks at 7085, 6834 and 6541 cm^{-1}, an argument was put forward to associate those absorption bands with S_0, S_1 and S_2 form, respectively. Once those assignments were made, we proceeded to calculate the relative contribution (%) of each form of hydrogen bonding, S_i, (where i=0,1,2) and the ratio of hydrogen bonded to the total absorbed water, S_t (where $S_t = S_0 + S_1 + S_2$). It is assumed that S_i/S_t is proportional to C_i/C_t, where C is the concentration given as C=A/a, A is the area under the absorption peak and a is the absorption coefficient. As a first approximation, the literature values of absorption coefficients a_0, a_1 and a_2 were used for S_0, S_1 and S_2 forms, respectively. Equation 4.2.1.3 was then used to calculate the relative concentration of each species:

Equation 4.2.1.3
$$\frac{C_i}{C_t} = \frac{S_i}{S_t} = \frac{A_i/a_i}{A_{7085}/a_0 + A_{6834}/a_1 + A_{6541}/a_2}$$

The relative ratio of various forms of absorbed water is plotted as a function of water content in Figure 4.2.1.19. It is interesting to note that about 30% of the absorbed water is in the S_0 form, 50% in the S_1 form and 20% in the S_2 form. Note also that the ratio of any absorbed species (S_i) to the total absorbed water (S_t) varies little with moisture content (%). We reiterate that the S_0 form represents a water molecule that does not form

51

hydrogen bonds through either of its hydrogen atoms but can do so through its oxygen atom. We also acknowledge the work by Weir et al.[4] who used UV reflection spectroscopy to study water-epoxy interactions, though their method was limited to the detection of water-SO_2 interactions.
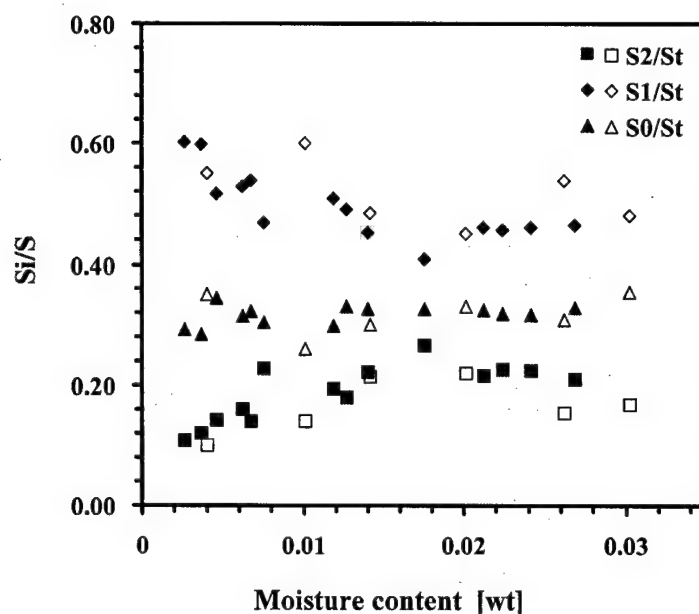
Figure 4.2.1.19 Relative ratio of the three forms of absorbed water (S_0, S_1 and S_2) to the total water content (S_t) as a function of moisture content. Solid symbols represent NIR results, open symbols the results from molecular simulations.

Finally, molecular simulations were conducted in order to provide additional molecular level insight into the water-network interactions in our systems.[2] In recent years, simulation studies have revealed interesting information about molecular structure of water and adhesives. Examples include, but are not limited to, the studies of the dynamics of pure water,[5] crystallization of water,[6] molecular dynamics of water-polymer solutions,[7] simulations of structure and properties of cross-linked resins,[8] molecular dynamics of tethered chains in polymer melt adhesives.[9] Here, however, we report for the first time a molecular simulation study of hydrogen bonded states of water molecules absorbed in a thermoset network adhesive. For more detailed description of our procedure the reader is referred to the experimental part; in sum, however, the amorphous cell containing a stoichiometric DGEBA-DETA network together with a select number of water molecules was subjected to a thermal history that parallels the experimental conditions and the final structure was recorded and studied. A hydrogen bond count was conducted based upon two criteria:[10] 1) the distance between the proton and the acceptor is shorter than 2.4 Å, and 2) the donor-proton-acceptor angle is greater than 145°. Our principal findings are as follows. It was established that a water molecule could: 1) form a hydrogen bond with hydroxyl oxygen, ether oxygen and/or tertiary amine nitrogen of the polymer network; 2) form a hydrogen bond with another water oxygen, and 3) act as a hydrogen bond acceptor for hydroxyl hydrogen of the polymer network. The majority of absorbed water molecules reside in the network as single molecules, and that is true at all levels of water content. Dimers are first found at the water content of 0.4% (by wt.); trimers appear at about 1.4% and clusters of four water molecules at above 2.0%. A larger cluster (involving six water molecules) was found only once in over 70 simulations.

We emphasize that in the trimers and clusters observed in our study, water molecules were linked through hydrogen bonds but did not necessarily form cyclic structures that have been reported in the simulation studies of liquid water. Of all S_0 molecules, about two thirds formed hydrogen bonds through the oxygen atom. If the one third of S_0 molecules that did not form hydrogen bonds are considered as "free water" then its total amount stands at about 10%. That number is larger than the estimate obtained from the DRS data (ca. 5%), but considering the assumptions involved and the precision limit of the measurements, the observed agreement is excellent.

The images of S_0, S_1, and S_2 forms generated by simulation are illustrated in Figure 4.2.1.20, in which hydrogen bonds appear as dashed lines. Figure 4.2.1.20 a shows an example of the S_0 water molecule located in the center of the figure (oxygen is red, hydrogens are white). Note that neither of its hydrogens forms a hydrogen bond with the network, while its oxygen bonds to the hydroxyl group of the network. Figure 4.2.1.20 b shows an example of the S_1 form; here, the water molecule in the center of the figure forms one hydrogen bond, in this case with the hydroxyl oxygen of the glycidyl group. Figure 4.2.1.20 c shows an example of the S_2 form in which both hydrogens form bonds with the network.

The results obtained from molecular simulations were quantified and used to calculate the relative contribution (%) of each form of hydrogen bonding, S_i, (where i=0,1,2) and the ratio of hydrogen bonded to the total absorbed water, S_t (where $S_t = S_0 + S_1 + S_2$). A comparison of the NIR results with the results from molecular simulations is illustrated in Figure 4.2.1.19. The observed agreement between the two techniques regarding the relative contribution of each form of hydrogen bonding is excellent.
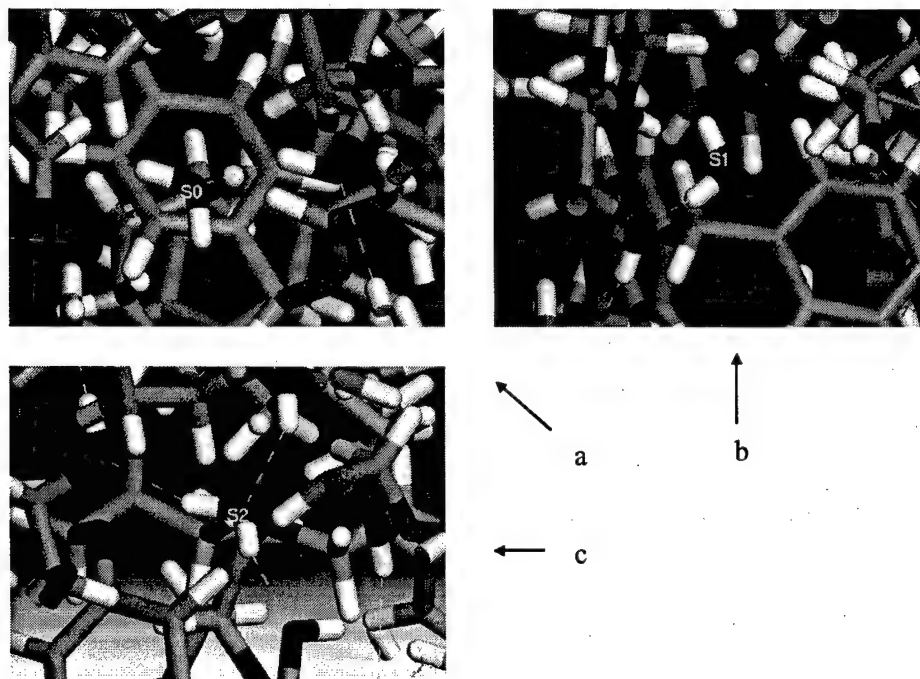
Figure 4.2.1.20 Snapshots from the results of molecular simulations showing three different forms of water molecules in the network: a) the S_0 form; b) the S_1 form; and c) the S_2 form.

4.2.1.2.2 Two-Dimensional (2D) DRS study of the water absorption of DGEBA-DETA system[11]

Two-dimensional (2D) DRS was also applied to study the influence of short time water exposure on the stoichiometric DGEBA-DETA network. The basic concept of constructing 2D spectra from the perturbation-induced fluctuations of one-dimensional (1D) spectra was first introduced by Noda in 1986.[12] In that pioneering work, the external stimulus was limited to a simple sinusoidal waveform with a fixed frequency. In 1993, Noda generalized his formalism to perturbations characterized by an arbitrary waveform.[13] Since then, the 2D correlation analysis has been applied to a host of spectroscopic techniques that include IR,[14-16] Near-IR (NIR),[17] Raman,[14] UV-visible,[18] Fluorescence[19] and NMR.[20,21] An overview of 2D correlation spectroscopy is found in references [22] and [23]. The most important advantages of 2D over 1D spectroscopy are: 1) the possibility of improving the resolution and enhancing the separation of overlapping molecular events; and 2) the possibility of probing the relative rate of spectral intensity changes during the application of an external stimulus. The 2D spectra appear particularly promising in the studies of polymer dynamics where a precise identification of molecular mechanisms with different time and length scales is often the key goal.

A 2D analysis requires that the external stimuli (varying water content in our case) be equally spaced and our DRS spectra were adjusted accordingly by linear interpolation. "2D Pocha" software by Daisuke Adachi (Kwansei Gakuim University) was used in the analysis.

The 1D DRS spectra (dielectric loss in the frequency domain) of a DGEBA-DETA network with different water content are shown in Figure 4.2.1.13. We observe a

broad relaxation peak in the dry network which increases with increasing water content. The solid lines in Figure 4.2.1.13 are composite fits of the dc conductivity term and two Cole-Cole functional forms that describe two relaxation processes (termed β and γ, respectively, in the order of increasing frequency), as shown in the inset of Figure 4.2.1.13. The dielectric relaxation strength of β and γ processes, obtained from the fits, is shown as a function of water content in Figure 4.2.1.21; note that the β process increases faster than the γ process.

In the text below we refer briefly to the salient features of the 2D correlation analysis. Two types of spectra can be obtained from a 2D correlation analysis, synchronous and asynchronous. The synchronous 2D correlation spectrum reflects a simultaneous change in spectral intensities at two different frequencies, while the asynchronous spectrum depicts a sequential change. The synchronous and asynchronous 2D DRS spectra of our networks were generated from the data in Figure 4.2.1.13 and are shown in Figure 4.2.1.22 a and b, respectively. The color scale represents the correlation intensity, which increase from negative (blue) to zero (light green) to positive (red). The synchronous spectrum (Figure 4.2.1.22 a) is symmetric with respect to the diagonal line and the correlation peaks appear at both diagonal (autopeaks) and off-diagonal (cross-peaks) positions. The autopeaks identify the signals that undergo changes with the external stimulus and are always positive. The cross-peaks, on the other hand, are positive if the two signals change in the same direction (either increase or decrease) and are negative otherwise. In the synchronous spectra of Figure 4.2.1.22 a, we observe one autopeak (10^1, 10^1 Hz) and two crosspeaks (10^{-2}, 10^1 Hz) and (10^1, 10^{-2} Hz). All those peaks are positive, which signifies that the measured parameter (dielectric loss) changes

in the same direction with water content at all frequencies. In this case, based on the underlying physics, we know that the dielectric loss in the frequency domain *increases* with increasing water content.
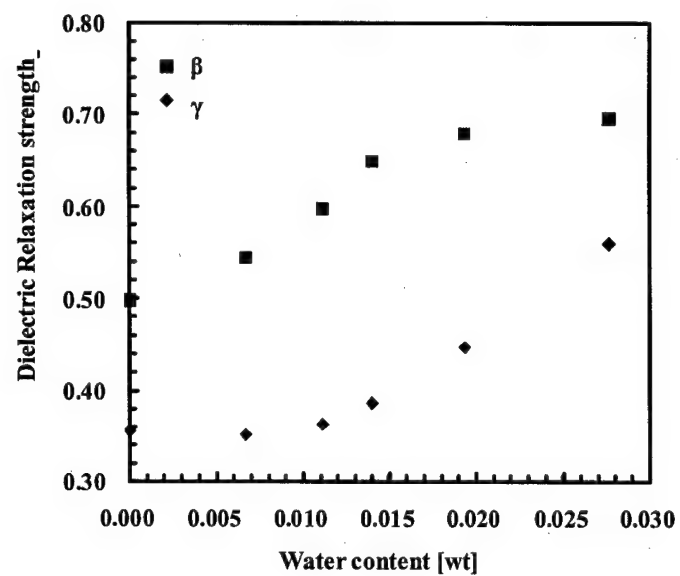
Figure 4.2.1.21   Dielectric relaxation strength of β and γ processes as a function of moisture content, measured at -60°C.
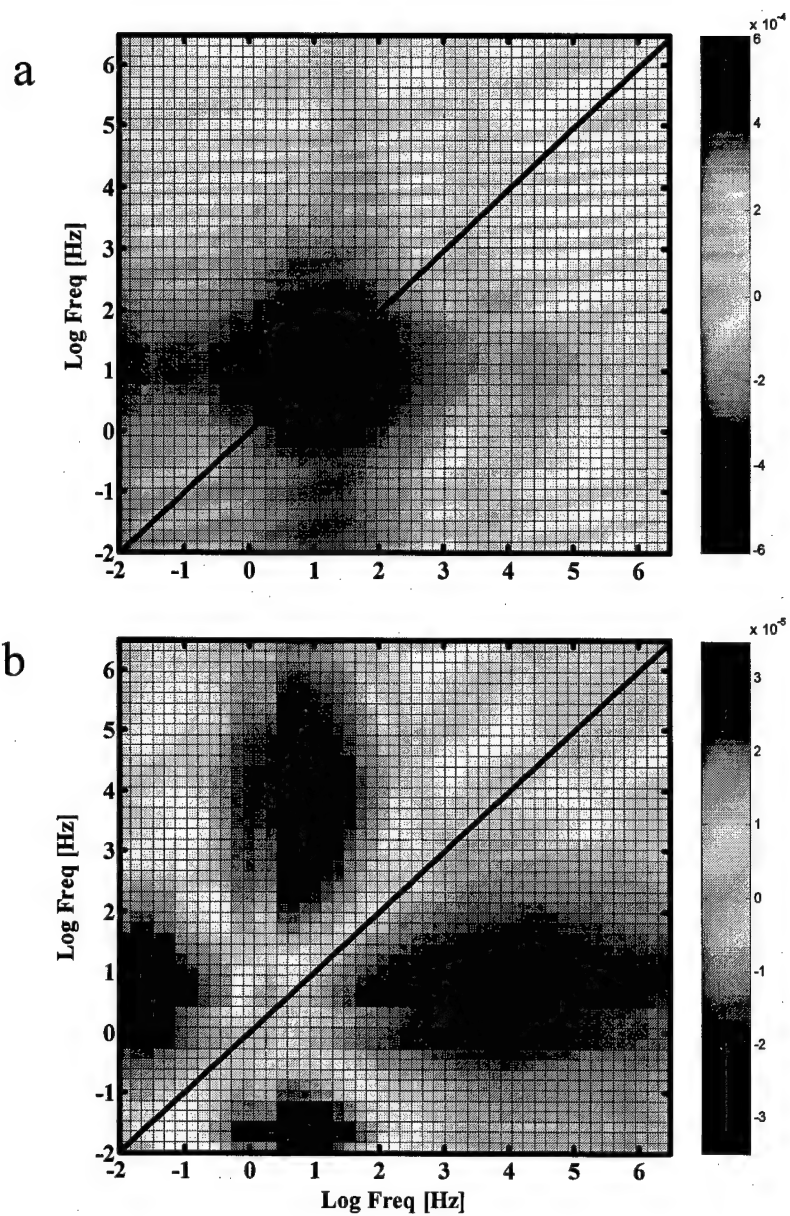
Figure 4.2.1.22 Synchronous (a) and asynchronous (b) 2D correlation DRS spectra.

The asynchronous spectrum has a better resolution than the synchronous spectrum. Recall that the asynchronous correlation spectrum contrasts spectral intensities at two frequencies that change at different rates. The asynchronous spectrum is antisymmetric and contains no autopeaks but only cross-peaks at off-diagonal positions that appear when two dynamic spectral intensities are out of phase (either accelerated or delayed). A cross-peak with coordinates f_1 and f_2 is positive if the spectral intensity change at f_1 is accelerated with respect to that at f_2, and negative if the opposite is true. Let us focus on the upper left portion of the spectrum (above the diagonal line) in Figure 4.2.1.22 b. We can see two peaks, one negative peak at $(10^{-2}, 10^1$ Hz) and one positive peak at $(10^1, 10^4$ Hz). The negative value at $(10^{-2}, 10^1$ Hz) indicates that the rate of change of the process at 10^{-2} Hz is slower than that at 10^1 Hz. The positive value at $(10^1, 10^4$ Hz) means that the process at 10^1 Hz changes faster than that at 10^4 Hz. The absence of a peak at $(10^{-2}, 10^4$ Hz) implies that the two processes at 10^{-2} Hz and 10^4 Hz change at a similar rate. Thus the 2D DRS spectra reveal the presence of three processes that vary with water content, at 10^{-2}, 10^1, 10^4 Hz.

We next compare the information obtained from 1D and 2D analysis and draw the following principal conclusions. First, the hypothesis based on the 1D fits that the loss spectra comprise a charge migration process and two relaxation processes is corroborated by the 2D analysis. The three processes at 10^{-2}, 10^1 and 10^4 Hz are clearly observed and identified with charge migration, β relaxations and γ relaxation, respectively. Second, the 2D analysis reveals that the process at 10^{-2} Hz (charge migration) changes slower than that at 10^1 Hz (β relaxation), which could not be clearly deduced from the 1D spectra. Third, the 2D analysis confirms that the process at 10^1 Hz (β) changes faster than that at

10^4 Hz (γ), in agreement with the 1D findings (Figure 4.2.1.21). And finally, the 2D analysis also reveals that charge migration and γ relaxation change at a similar rate with increasing water content; another observation that could not be made from the 1D spectra.

In sum, 2D correlation method was used for the first time in the analysis of relaxation processes in polymer networks. DRS is a powerful tool for the study of dynamics of solids (crystalline and amorphous), liquids and gases, and the utilization of the 2D analysis adds a new dimension to this technique that should prove informative for the characterization of relaxation processes with different time and length scales. We anticipate an increased use of the 2D DRS analysis in the near future.

4.2.1.2.3 Model System II ---- DGEBA-TEPA system

Figure 4.2.1.23. shows the dielectric spectra of the DGEBA-TEPA system with exposure time as a parameter, measured at –60°C. Note that the sub-Tg relaxation increases steadily with aging time, much like in the DGEBA-DETA system.
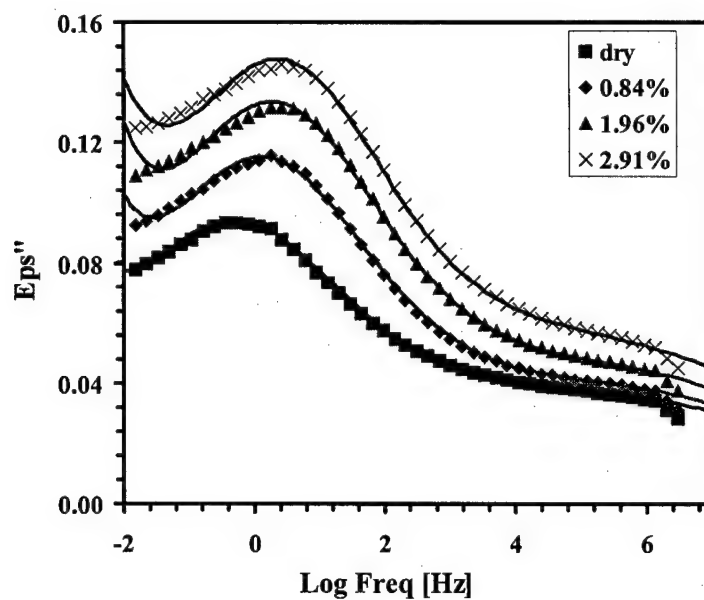
Figure 4.2.1.23 Dielectric loss in the frequency domain for 1E:1A DGEBA-TEPA network with moisture content as a parameter, measured at –60$^{\text{O}}$C.

4.2.1.3   Long Time Exposure

4.2.1.3.1 Model System I ---- DGEBA-DETA system

4.2.1.3.1.1   65°C Immersion Aging

As described in the experimental section, two exposure conditions were used: 65°C water immersion and 100°C water immersion. The results obtained following the 65°C aging are described first.

Gravimetric analysis

The data presented in Figure 4.2.1.24. show the water uptake profiles for three samples aged in deionized water at 65°C. There is a steady increase in water content within all joints during the first 10 days (15 on the scale shown). After that point we observe a continuing increase in water content in one sample (joint 26) and a slight reduction in the weight followed by an increase in mass in another sample (joint 27). Joint 29 however, exhibits a decrease in mass with aging time in excess of 10 days, suggesting that degradation had occurred within the adhesive or the joint. The observed weight loss may be related to the leaching of the adhesive, e.g. of the unreacted monomer units, or may occur as a result of chain scission within the epoxy matrix. Further aging shows that joint 27 begins to exhibit a similar feature to joint 29 after 35 days. At that point all joints were dried at 65°C to remove the absorbed moisture, determine the amount of weight loss in each sample and observe a (possible) recovery in the dielectric behavior of these samples. Upon drying, all joints showed a decrease in weight between 3 and 6 percent. It should be also noted that the aluminum adherends showed initial signs of corrosion on the outside (adherends had become dark and showed some powdery

residue). Consequently, some of the measured weight loss might be attributed to this phenomenon (the samples had to be lightly abraded to provide a contact for the dielectric measurements).

Dielectric analysis

In addition to the gravimetric analysis, the bonded joints were also monitored dielectrically, at room temperature and over the frequency range from 0.1Hz to 10^9Hz. Figure 4.2.1.25. shows the dielectric results obtained throughout the aging period of joint 26.

Looking at the upper plot (permittivity) first, we see a steady increase in dielectric permittivity during the first 336 hours as a result of moisture uptake. The high permittivity values present at low frequencies (below 10 Hz) may be attributed to the electrode polarization. Water is a polar molecule and thus an increase in the number of water molecules within the epoxy matrix will result in an increase in permittivity. After 336 hours the permittivity reaches a maximum and then decreases with further aging. This is in contrast with the results of the gravimetric study, which indicates (for this particular sample) continuing absorption. This is probably due to some degradation and leaching of dielectrically active species or due to dimensional changes, i.e., the thickness of the joints increases with water uptake, so that the measured permittivity is underestimated. Upon drying for 24 hours, the permittivity exhibits higher values than in the unaged joints, suggesting that some moisture is still present in the adhesive. Further drying (48 hours) results in a decrease in the permittivity with respect to the unaged values, again possibly due to the degradation/leaching of the adhesive and/or the increase

in thickness. Continued drying at 65°C up to 204 hours resulted in no significant change in permittivity.

The changes in the dielectric loss parallel the changes in permittivity. The loss increased steadily with the ingress of water for the first 336 hours. The high loss values at low frequencies come from the ionic conduction. The loss peak at 7000Hz is associated with the relaxation of hydroxyl groups; the increase in the intensity of this peak may be attributed to water hydrogen bonded to the pendant hydroxyl groups (more on that will be said in section 4.2.4 on molecular dynamics). In addition, the peak position, and hence the relaxation time of the β process, is shown to shift to higher frequencies with increasing water content, as a consequence of changes occurring in the local environment. After 336 hours in water at 65°C the loss begins to decrease with further aging. Upon drying for 24 hours, the dielectric loss has a higher value than in the unaged joint. Still further drying (48 hours) results in a decrease in the loss with respect to the unaged samples (again, similarly to the trend in permittivity). The higher loss values at lower frequencies in the spectra of redried samples may be due to the changes in the aluminum/adhesive interface as a result of water penetration.

Figure 4.2.1.24 Water uptake profiles of DGEBA-DETA joints during 65°C water immersion
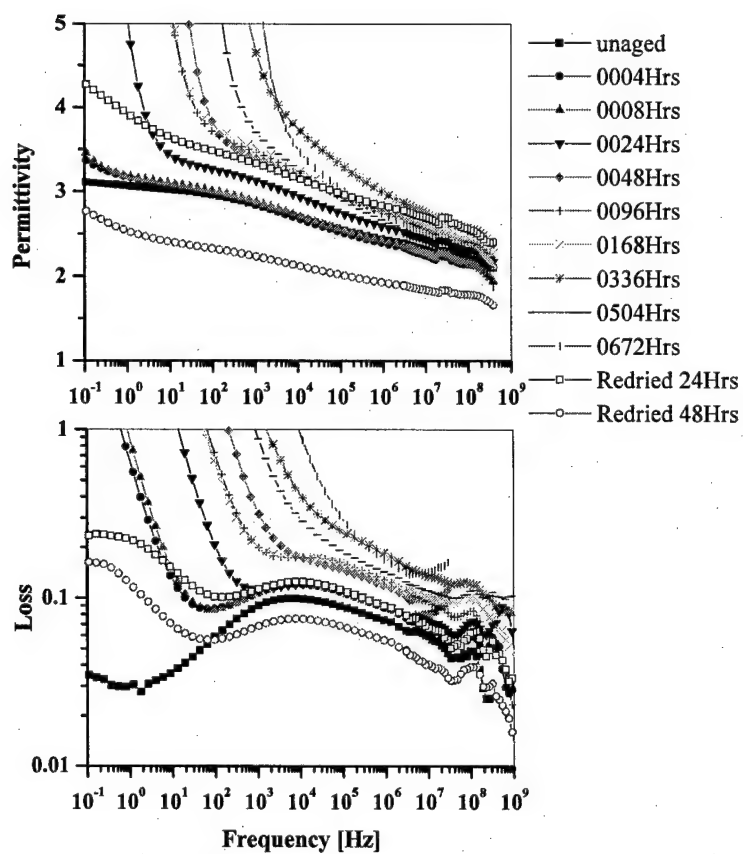
Figure 4.2.1.25 Dielectric spectra of DGEBA-DETA joints during 65°C water immersion with aging time as a parameter.

o100°C Immersion Aging

Next, we describe the results of 100°C water immersion experiments. Measurements were carried out over the frequency range from 0.01 Hz to 10^9 Hz and a temperature range from -100°C to 60°C.

Gravimetric analysis

Figure 4.2.1.26. shows a typical water uptake profile for samples exposed to deionized water at 100°C up to 3517 hours. At tat time we stopped to record the weight because we needed to abrade the surface of the adhesive joint to obtain good contact in dielectric measurements. It appears that the observed increase in the moisture content with exposure time can be divided into roughly four stages. These four stages are: I) exposure time <287 hours (16.9 on the scale), water content increases steadily with exposure time; II) 287 hours< exposure time <676 hours (26 on the scale), water content reaches a plateau; III) 676hours< exposure time<1911 hours (43.7 on the scale), water content increases again with exposure time; IV) 1911hours< exposure time, water content reaches another plateau. The maximum water content is 6.5%, higher (as expected) than the value obtained in the 65°C aging experiments. This maximum value is also higher than that obtained following exposure to 80°C/98%RH (in Section 4.2.1.2.1). The observed difference results from the difference in the aging time and temperature. It is also interesting to note that the maximum water content measured last year was about 3.0%, not far from the value of the first plateau in Figure 4.2.1.26.

Dielectric analysis

Dielectric relaxation spectra over a wide range of frequency (0.01Hz to 10^9Hz) and temperature (-100°C to 60°C) were collected at all stages of water absorption. Figure 4.2.1.27. shows the dielectric relaxation spectra in the frequency domain measured at −

70

100°C with aging time shorter (a) and longer (b) than 676 hours. Similar trends were observed at other temperatures.

Dielectric loss increases with exposure time shorter than 676 hours; after that, a new loss peak (at 10Hz) appears and increases with aging time until about 2450 hours. Besides that new peak, the loss spectra do not change much, suggesting that only the new process changes with aging time in this stage. We term this new relaxation – the δ process. The time at which the δ process first appears is close to the onset of the second increase in water content and hence it is possible that the δ process is related to that stage of water absorption. The mechanism of this relaxation is not completely understood at present; however, it is unlikely that the δ process is related to the β process which enters our frequency window at temperature higher than −90°C.

Figure 4.2.1.28. shows the dielectric spectra of the sample exposed to 100°C water for 3517 hours and measured over a temperature range from −100°C to 60°C. Note that after such long exposure to water, the β process could not be separated out because of the high ionic conductivity, while the δ process is seen clearly. The molecular origin of the δ process is under investigation.
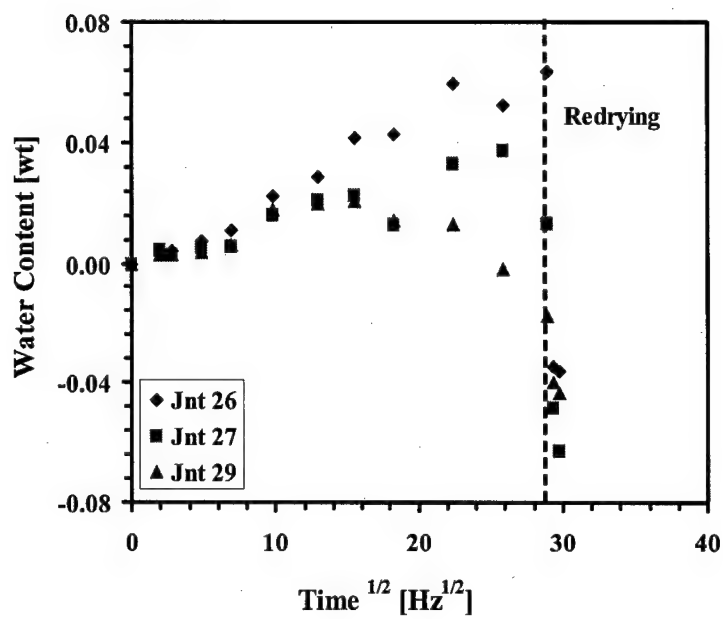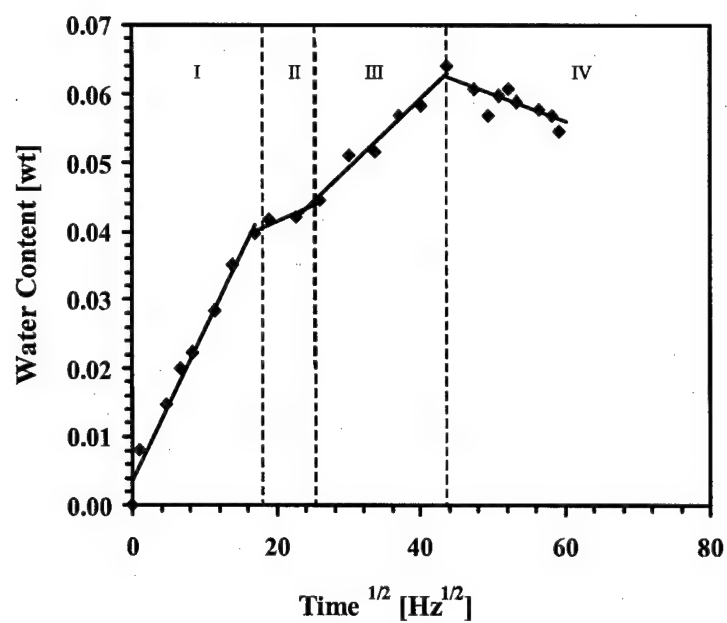
Figure 4.2.1.26 Water uptake profile of DGEBA-DETA joints during 100°C water immersion
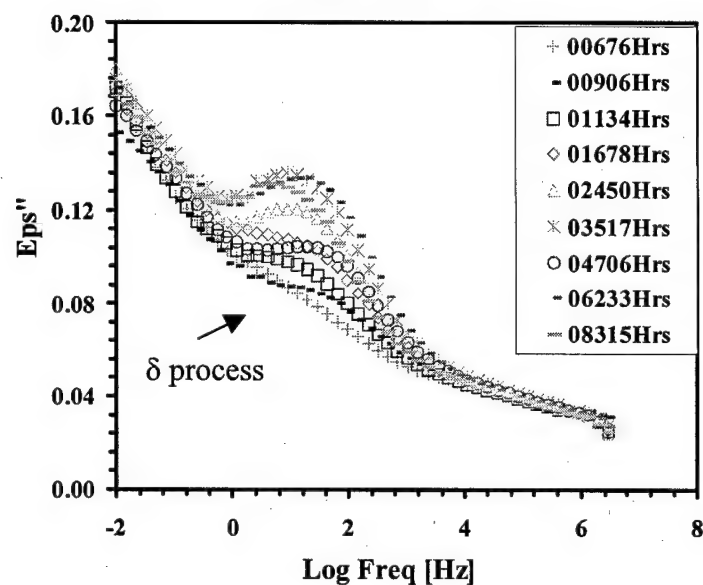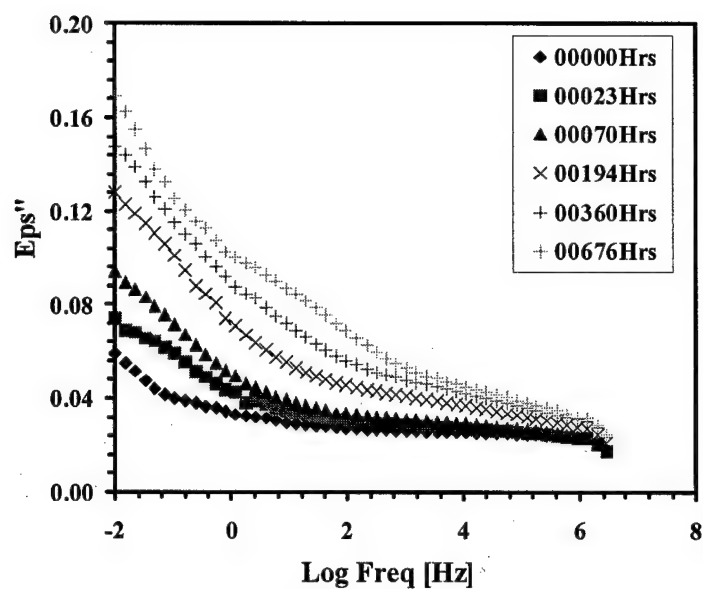
Figure 4.2.1.27 Dielectric spectra of DGEBA-DETA samples measured at −100°C with aging time shorter (a) and longer (b) than 676 hours.
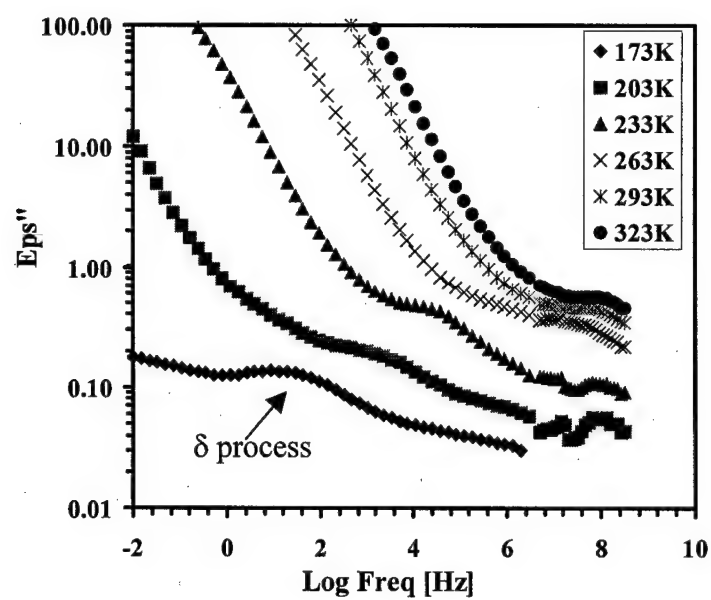
Figure 4.2.1.28 Dielectric spectra of DGEBA-DETA sample aged in 100°C water for 3517 hours with measuring temperature as a parameter..

The quantification of the DRS data was performed based on the 203K measurements, because it encompasses β, γ and δ processes. For the exposure time shorter than 360 hours, two relaxation processes could be readily deconvoluted; when the exposure time exceeds 360 hours, the emergence of the δ process adds three more unknowns (relaxation strength, relaxation time, Cole-Cole parameter). To obtain a reliable fit, we fixed all parameters of β and γ processes for exposure time longer than 360 hours. The fitting results are as follows:

Cole-Cole parameters

For β and γ processes, we set

Equation 4.2.1.4 $\qquad\qquad\qquad a_\beta = 0.354$

Equation 4.2.1.5 $\qquad\qquad\qquad a_\gamma = 0.160$

The Cole-Cole parameters for the δ process are scattered (shown in Figure 4.2.1.29), without an obvious trend.

Frequency at maximum loss

Figure 4.2.1.30 shows frequency at maximum loss as a function of the moisture contents and/or exposure time.

Dielectric Relaxation strength

The relaxation strength of β, γ and δ processes as well as low frequency limiting dielectric permittivity (ε_0) as a function of water content and exposure time is shown in Figure 4.2.1.31.
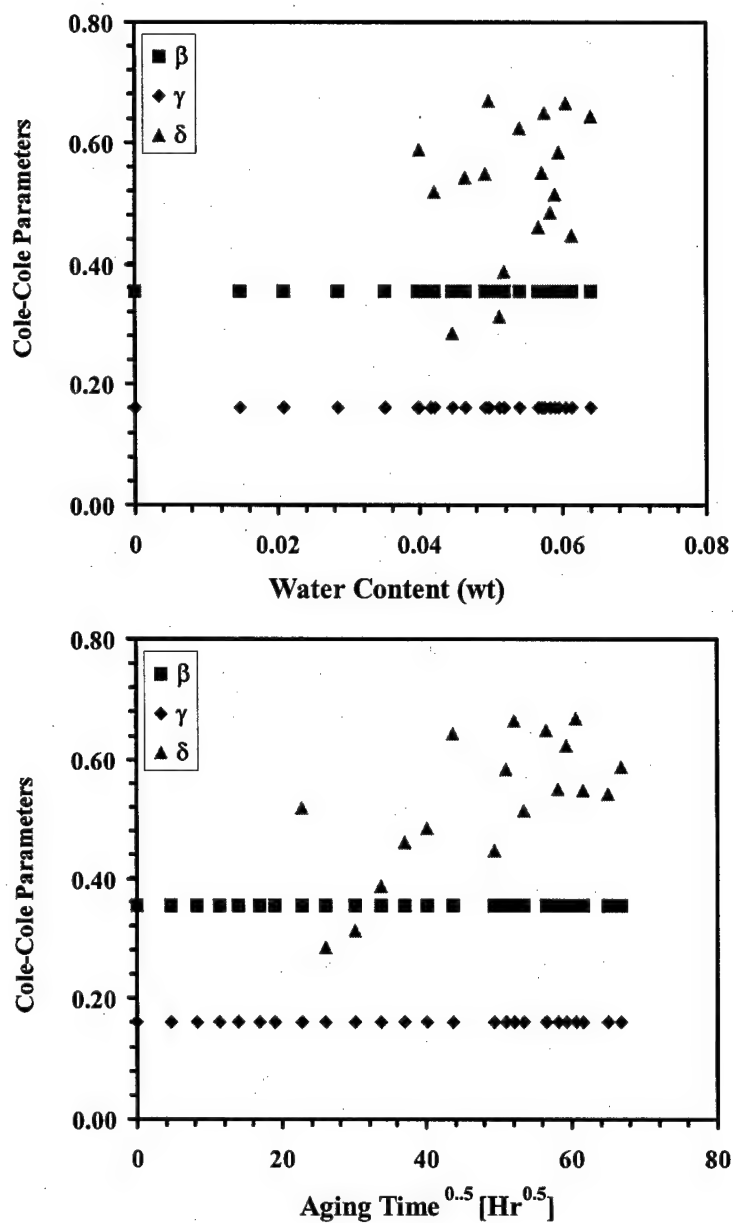
Figure 4.2.1.29 Cole-Cole parameters of β, γ and δ processes of DGEBA-DETA system as a function of water content (upper figure) and aging time (lower figure).
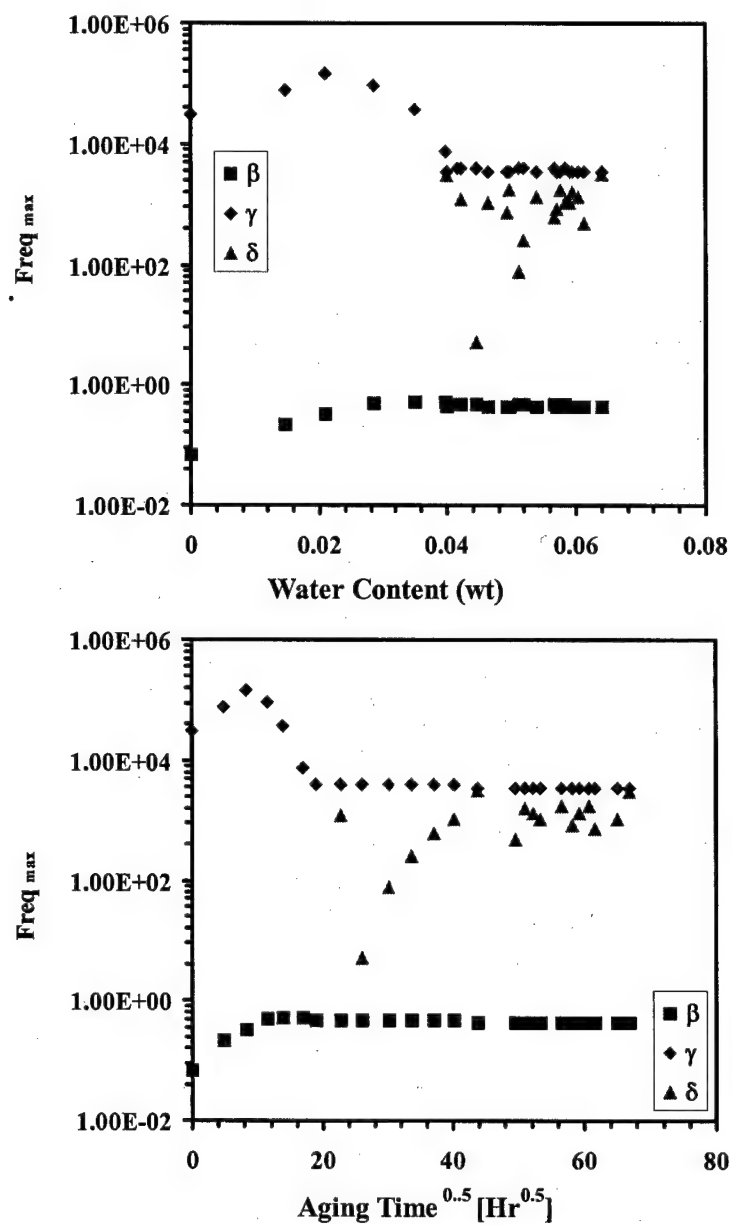
Figure 4.2.1.30   Frequency at maximum loss of β, γ and δ processes in DGEBA-DETA system as a function of water content (upper figure) and aging time (lower figure).
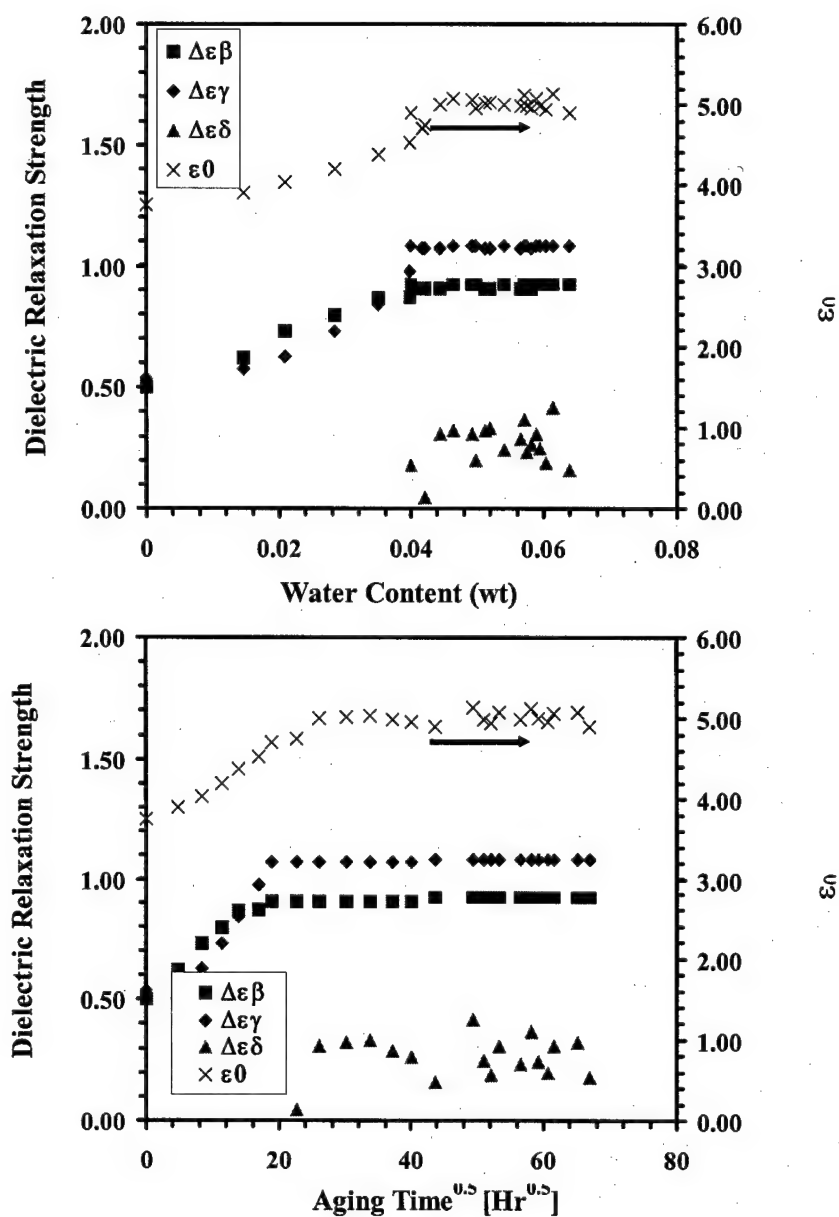
Figure 4.2.1.31   Relaxation strength of β, γ and δ processes in DGEBA-DETA system as a function of water content (upper figure) and aging time (lower figure).

The effects of redrying

After immersion in 100ºC boiling water for 10262 hours, the sample was redried at 100ºC until its weight did not change any more. A comparison of the dielectric loss spectra of dry and redried sample is shown in Figure 4.2.1.32. We see that: 1) the δ peak disappears, 2) the relaxation strength of the redried sample is lower than that of the dry sample; and 3) the relaxation time of the redried sample is longer than that of the dry sample, as detailed in Figure 4.2.1.33. From Figure 4.2.1.33, we see that both β and γ processes are slowed down after immersion and redrying. The activation energies for β and γ processes increased from 68 and 48 kJ/mol to 76 and 51kJ/mol, respectively, after aging and redrying. The changes in relaxation time and activation energy indicate that aging and redrying yield a denser network, possibly due to chemical reactions.
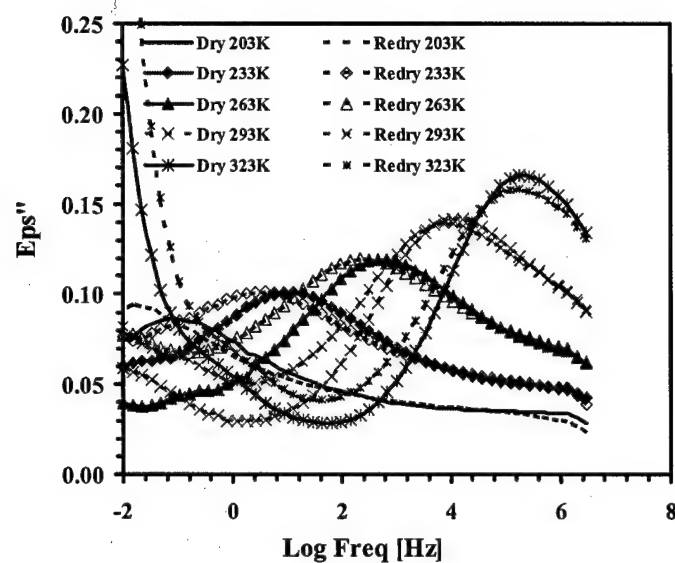
Figure 4.2.1.32 Comparison of dielectric loss spectra of dry and redried DGEBA-DETA sample, with measuring temperature as a parameter.
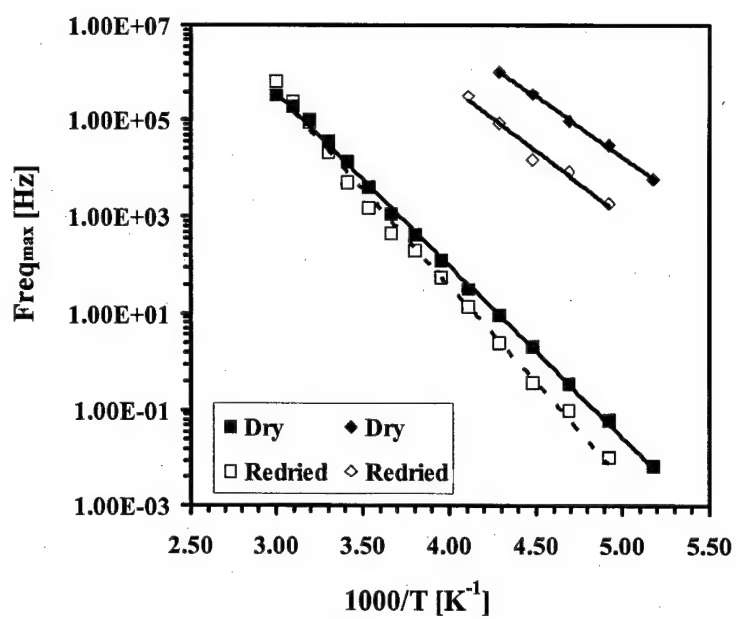
Figure 4.2.1.33 Comparison of frequency at maximum loss of dry and redried DGEBA-DETA sample as a function of reciprocal temperature.

4.2.1.3.2 Commercial System ---- Epibond 1590 system

4.2.1.3.2.1 65°C Immersion Aging

Gravimetric analysis

A typical water uptake profile for joints manufactured using Epibond 1590 is shown in Figure 4.2.1.34. It appears that a two-stage absorption process occurs at 65°C. The first stage (0 to 7 on the scale shown) is characterized by a steady increase in the water content and may be associated with the plasticization of the epoxy matrix. The second stage (7 to 13 on the scale shown) shows a dramatic increase in the water content in the adhesive and may be attributed to water entering the intermolecular space formed as a result of plasticization. The decrease in the water content observed after 240 hours (15 on the scale) is most likely due to degradation and subsequent leaching of the low molecular weight products. It should be noted that the maximum water content for this adhesive system is greater than that for the DGEBA-DETA system indicating a greater affinity for water; however, without mechanical testing the full extent of the degradation of the adhesive cannot be readily assessed.

Dielectric Analysis

Figure 4.2.1.35 illustrates typical permittivity and loss plots for those joints. We observe an increase in both permittivity and loss with aging time, associated with the ingress of water into the bonded structure. The high loss values at frequencies below 10 Hz may be attributed to the ionic conduction caused by the migration of various charge carriers.
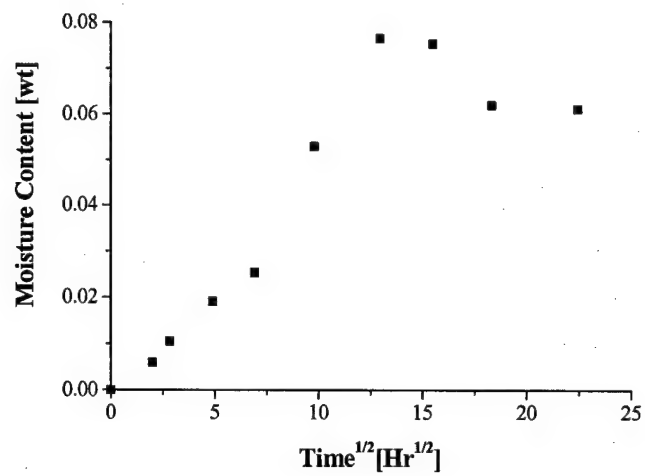
Figure 4.2.1.34 Typical water uptake profile for Epibond 1590 during 65°C water aging
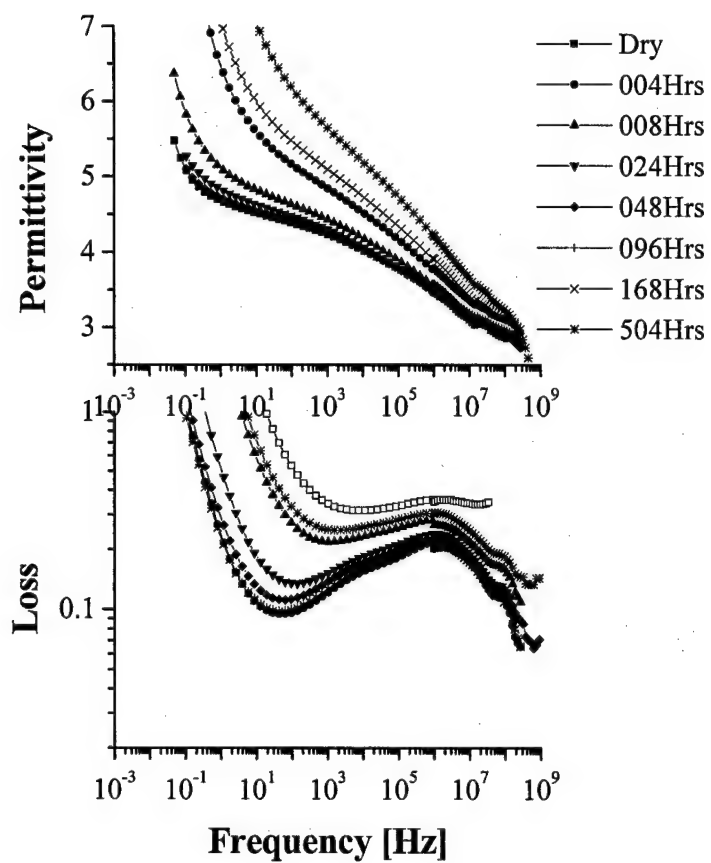
Figure 4.2.1.35 Dielectric spectra of Epibond 1590 during 65ºC water aging

4.2.1.3.2.2 100°C Immersion Aging

Gravimetric analysis

Figure 4.2.1.36 shows the water uptake profiles for Epibond joints aged at 100°C. It could be seen that at aging time shorter than 36hours (6 on the scale), there is a rapid and steady increase of water content with increasing aging time. After that, the rate of water absorption decreases gradually until water content reaches a plateau at 460 hours (22 on the scale). For aging times over 1600 hours (40 on the scale), the water content begins to decrease.

Dielectric analysis

Similarly to the DGEBA-DETA system, the aging of the Epibond joints in the 100°C water was also monitored dielectrically. Figure 4.2.1.37 shows the dielectric spectra of Epibond for exposure time shorter (a) and longer (b) than 36 hours, measured at –100°C. Dielectric loss increases gradually with aging time for the first 36 hours, after which a new relaxation appears in the spectra at roughly 1000Hz. This new relaxation continues to increase with aging time until about 620 hours. We term this new relaxation - the ω process. The permittivity and loss spectra did not change with aging time from 620 to 8304 hours, after which the sample was taken out of water environments and redried. It appears that the time when water content reaches a plateau (620 hours) corresponds to the time when permittivity and loss spectra cease to change with aging. However, although the dielectric spectra did not show obvious change, the gravimetric data show a decrease in water content at aging time longer than 1600 hours.

Figure 4.2.1.38 shows spectra of samples aged for 2126 hours at 100°C, with measuring temperature as a parameter. From this figure, we see that the ω process (see arrow) shifts from low to high frequency with increasing measuring temperature, while the original sub-Tg process relaxation could not be separated out because of the high ionic conductivity.

The origin of the new process was investigated by analyzing the effect of aging on the DRS spectra of pure resin (without the influence of the electrodes) as well as adhesive joints with different electrodes. We observe the ω process in all systems, including the neat resin, as well as the adhesive joints with copper and iron electrodes, as shown in Figure 4.2.1.39. This implies that the ω process has its origin in the interactions between water and neat resin.
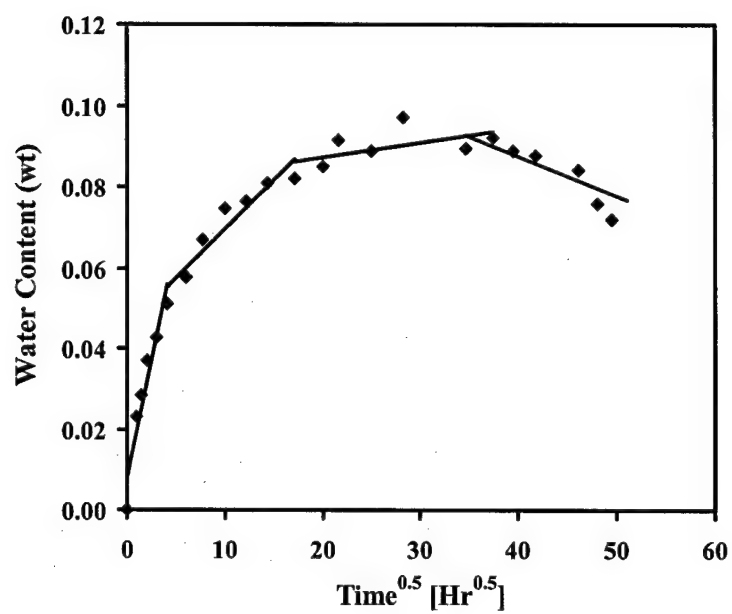
Figure 4.2.1.36 Water uptake profiles for Epibond joints aged at 100°C
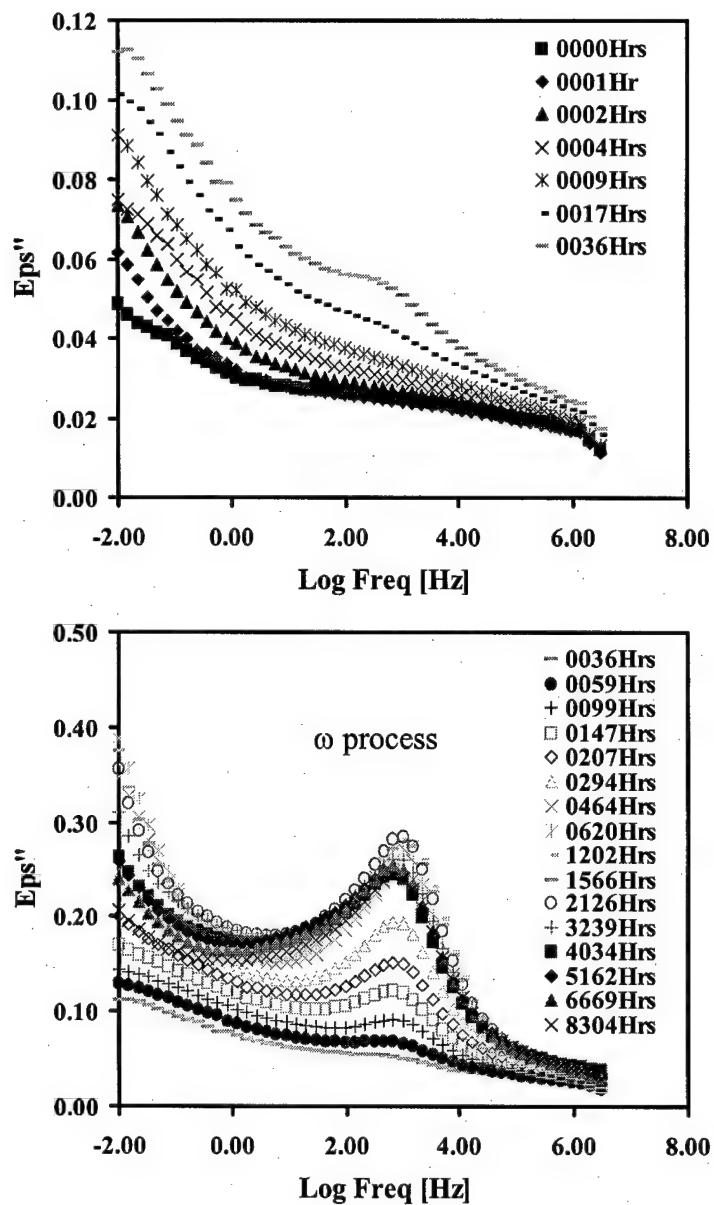
Figure 4.2.1.37 Dielectric spectra of Epibond system for aging time shorter (upper) and longer (lower) than 36 hours, measured at −100°C.
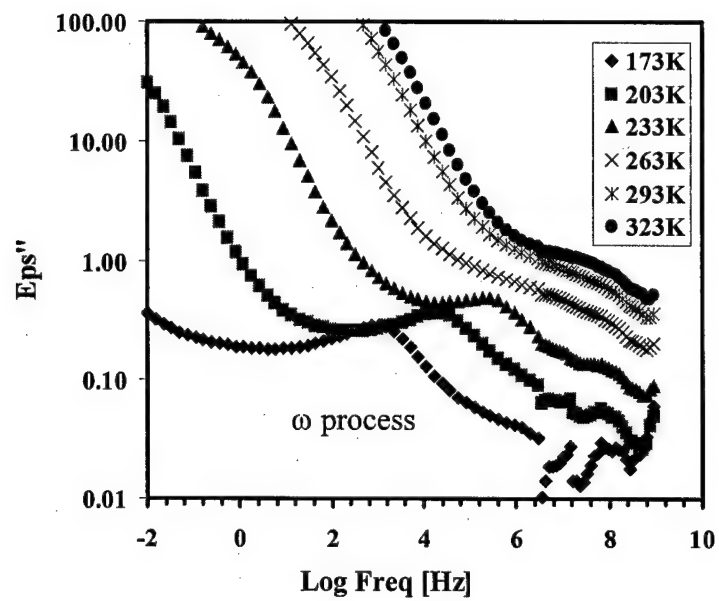
Figure 4.2.1.38 Dielectric spectra of Epibond system after 2126 hours aging.
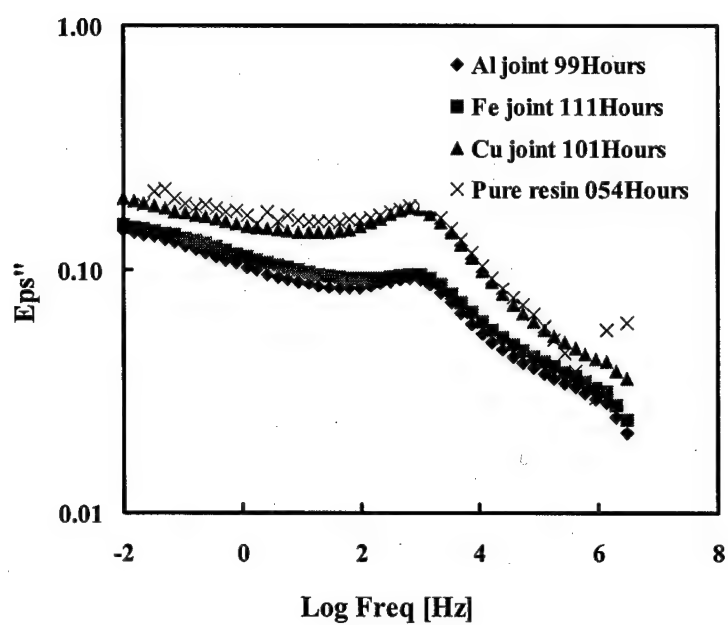
Figure 4.2.1.39 Dielectric loss spectra of Epibond system with aluminum, iron, copper and no adherends after 100 hours 100° C water immersion, the ω peak appears in all of the four systems.

The quantification of the Epibond DRS data was performed by fitting the spectra with three Cole-Cole functions. We choose 203K measurements because it encompasses β, γ and ω processes.

Cole-Cole fits

During fitting, the Cole-Cole parameters were fixed as follows:

Equation 4.2.1.6 $\qquad\qquad$ $a_\beta = 0.3700$

Equation 4.2.1.7 $\qquad\qquad$ $a_\gamma = 0.1850$

which means that both β and γ processes show no (or little) dependence on the moisture content. Compared with the δ process in the DGEBA-DETA system, the ω process has a higher Cole-Cole parameter of about 0.80 (Figure 4.2.1.40).

Relaxation Frequencies

The fitting results of relaxation frequencies for β, γ and ω processes are shown in Figure 4.2.1.41, as a function of exposure time and/or moisture content. We see that the β process speeds up, while the γ process slows down at the beginning of exposure and levels off when the ω process appears. The relaxation frequency of the ω process does not change appreciably with either exposure time or moisture content. The effect of water content (at less than 5%) on the relaxation times of β and γ processes is fitted with two linear equations shown in the lower part of Figure 4.2.1.41.

Relaxation strength

The relaxation strength of β, γ and ω processes as a function of exposure time and/or water content is shown in Figure 4.2.1.42. We can see that for exposure times shorter than 464 hours (21.5 on the scale), both β and γ processes increase steadily with exposure time and/or water content. When exposure time exceeds 464 hours, we observe

a leveling off of $\Delta\varepsilon$ for β and γ processes. As to the ω process, its relaxation strength increases with increasing exposure time and levels off at about 800 hours (28 on the scale).

Also shown in Figure 4.2.1.42 is the low (ε_0) frequency limit dielectric permittivity as a function of exposure time and/or water content. ε_0 levels off at exposure times longer than 800 hours.
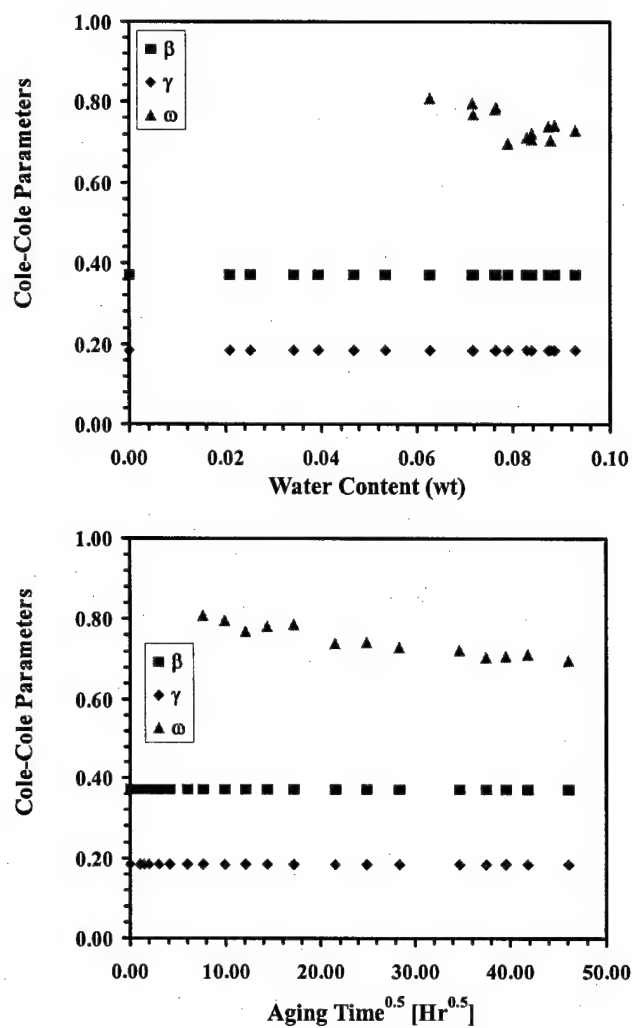
Figure 4.2.1.40 Cole-Cole parameters of β, γ and ω processes of Epibond 1590 system as a function of water content (upper figure) and aging time (lower figure).
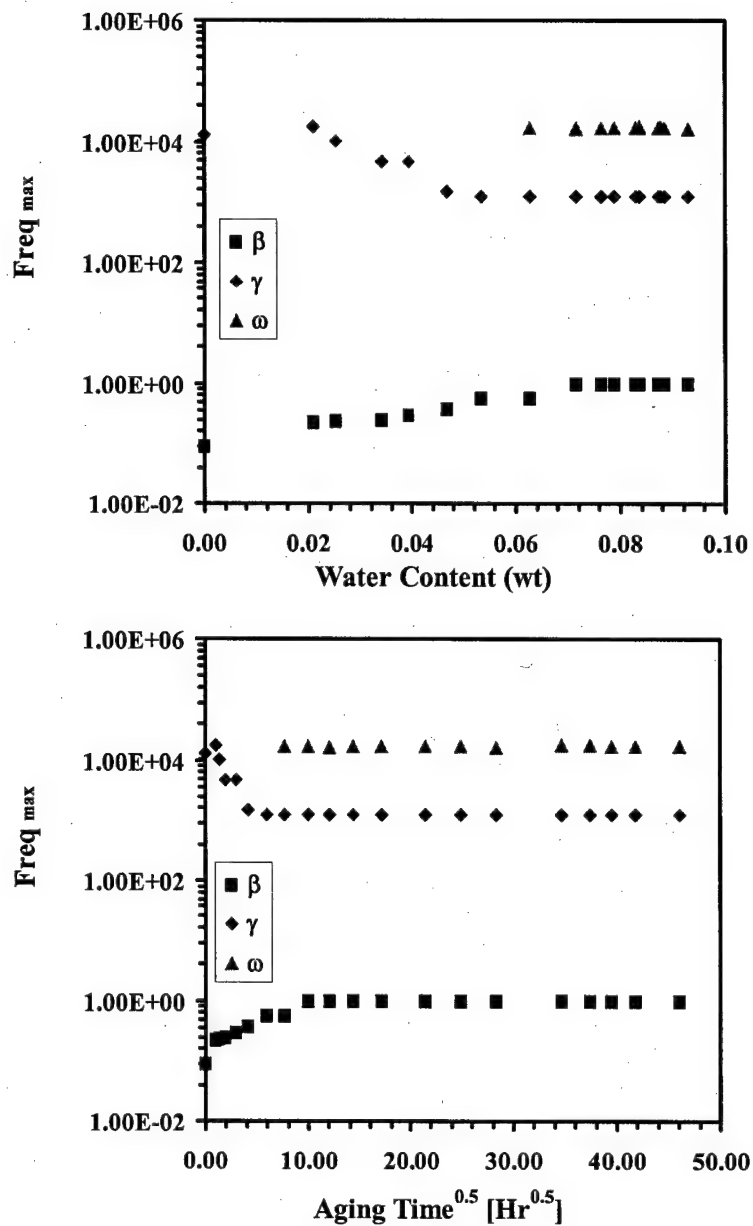
Figure 4.2.1.41 Frequency at maximum loss of β, γ and ω processes in Epibond 1590 as a function of water content (upper figure) and aging time (lower figure).

94
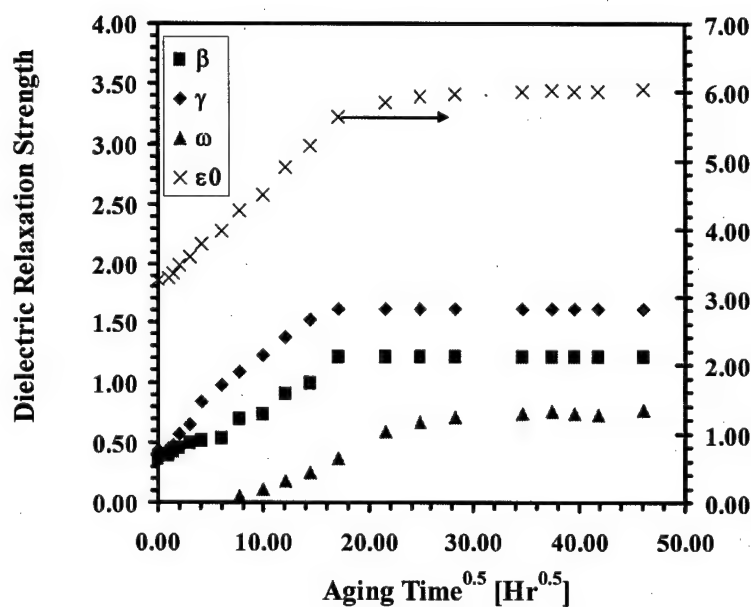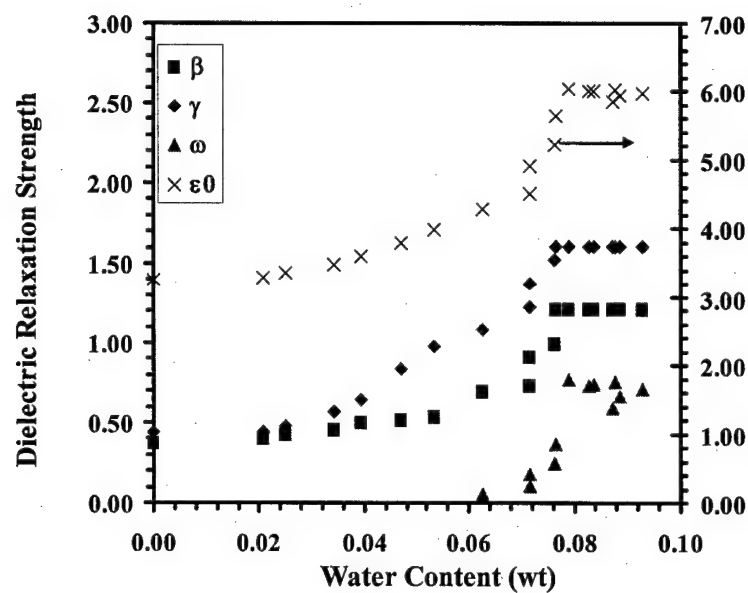
Figure 4.2.1.42   Dielectric relaxation strength of β, γ and ω processes as well as low frequency limit dielectric permittivity in Epibond 1590 as a function of water content (upper figure) and aging time (lower figure).

4.2.2 TDR

Experimental

Materials: DGEBA-DETA adhesive system is used; the description of the materials and curing conditions were given in section 4.1.1. We studied the effects of water exposure on the TDR traces of both "perfect" and "imperfect" joints. All joints had length of 130mm, width of 9mm and bondline thickness of 0.127mm. "Imperfect" sample had 1mm air gap in the middle of the adhesive joint.

Aging and Testing Conditions: Samples were aged by immersion in 100°C boiling water for selected time, followed by TDR measurements.

Equipment: same as in Section 4.1.2.

4.2.2.1 Perfect Joints

Figure 4.2.2.1 shows the TDR traces of "perfect" joint with aging time as a parameter, for immersion time shorter (a) and longer (b) than 200 days. Figure 4.2.2.1 (a) shows that in this time interval, the TDR traces shift to longer time, because the ingress of water slows down the velocity of the electromagnetic wave in the adhesive joint. However, after exposure to 100° C water for longer than 200 days, the TDR traces shift to shorter time, which may be the consequence of disbonding.

4.2.2.2 Imperfect Joints

Similar observation was made in "imperfect" joints, as shown in Figure 4.2.2.2.
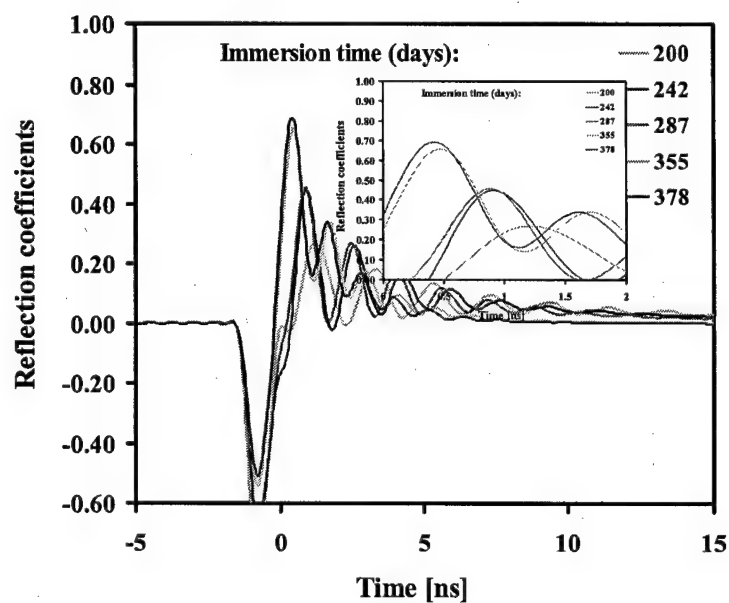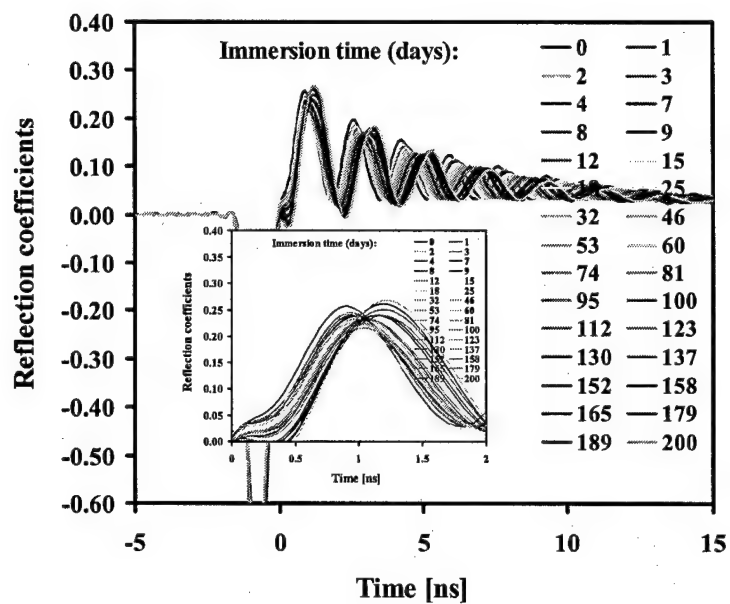
Figure 4.2.2.1 TDR traces of "perfect" joint for aging time shorter (upper) and longer (lower) than 200 days.
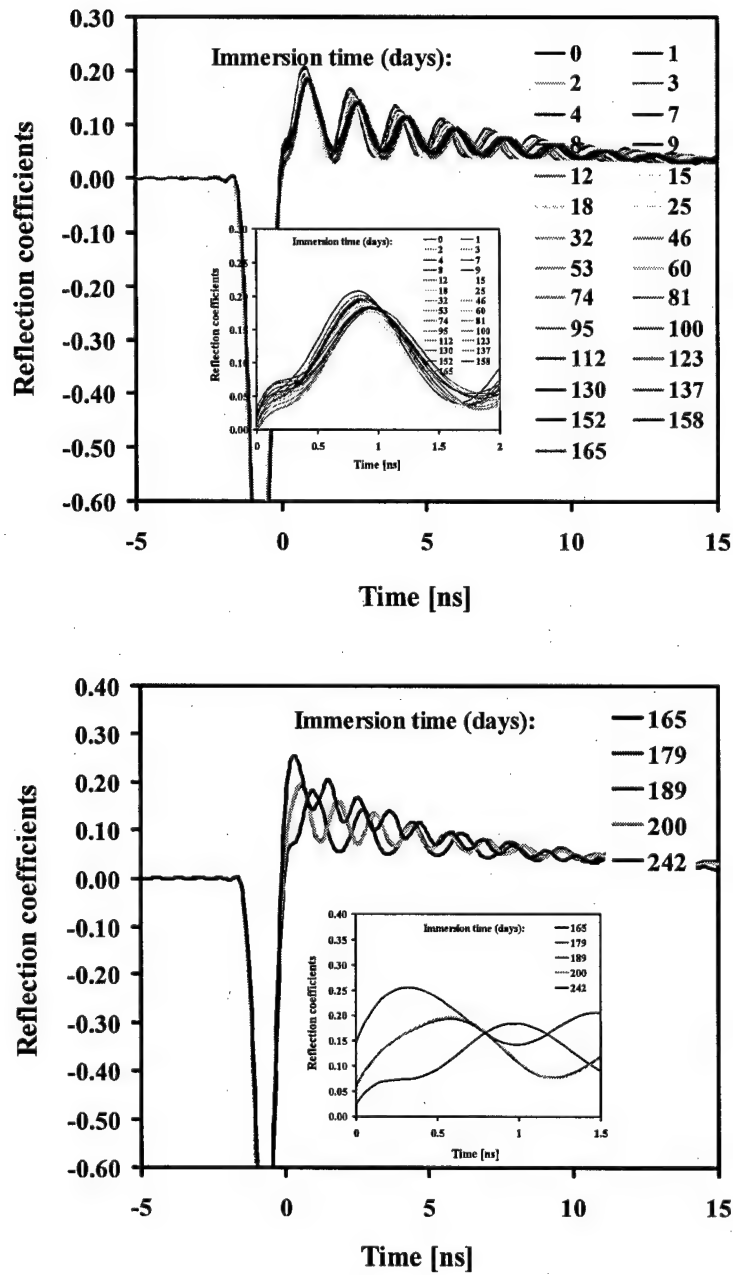
Figure 4.2.2.2 TDR traces of "imperfect" joint for aging time shorter (upper) and longer (lower) than 165 days.

4.2.3 Fiber Optic Near Infrared

4.2.3.1 Evanescent Mode

In section 4.2.1, we reported our initial finding that FT-NIR could provide molecular level information about the state of water in the adhesive. We were motivated by the complementary (to DRS) nature of the information obtained from the FT-NIR spectra. Consequently, we tried to implement the FT-NIR technique for in-situ fiber optic measurement of the state of water in the adhesive.

Optical fiber is composed of the glass core and the protective cladding. The latter has a lower refractive index than the core, so that the light can propagate through the core with little loss. When a small portion of the cladding is removed from the fiber, the infrared beam can probe the chemical state of the surrounding material and transmit that information by internal reflection to the detector. Our idea is to embed an optical fiber into the adhesive joint and use it for in-situ, real-time collection of FT-NIR spectra during moisture uptake.

Experimental

Materials: FT-600-EMT optical glass fiber, manufactured by 3M and obtained from ThorLabs, was used. De-ionized water, methanol and hexane were used as the media studied.

Testing Conditions: the experimental setup is shown in Figure 4.2.3.1. An 8-10cm length of cladding was stripped from the fiber. The fiber was passed through a beaker and fastened at the entrance and exit to prevent leaking. The fiber was connected

to the FT-NIR source and detector. The background was collected in an empty beaker. Then, the liquid was poured in and the spectra collected.

Equipment: Nicolet Instrument Magna 750 FTIR Spectrophotometer was used.

Results and Discussion

We studied the evanescent wave absorption spectra of liquid water, methanol and hexane, in order to prove the feasibility of the concept. Shown in Figure 4.2.3.2. are a spectrum of water with characteristic absorption peaks at $5200cm^{-1}$ and $7000cm^{-1}$, and the spectra of methanol and hexane with characteristic absorption peaks for carbon-hydrogen vibrations at $4335cm^{-1}$. The initial runs show that the signal is rather weak even though the spectra were obtained in pure liquids. In the adhesives, where only several percent (weight or volume) of water is typically absorbed, a higher sensitivity would be required.

From light source

500 ml beaker

Liquid studied

To detector

Fastening screw
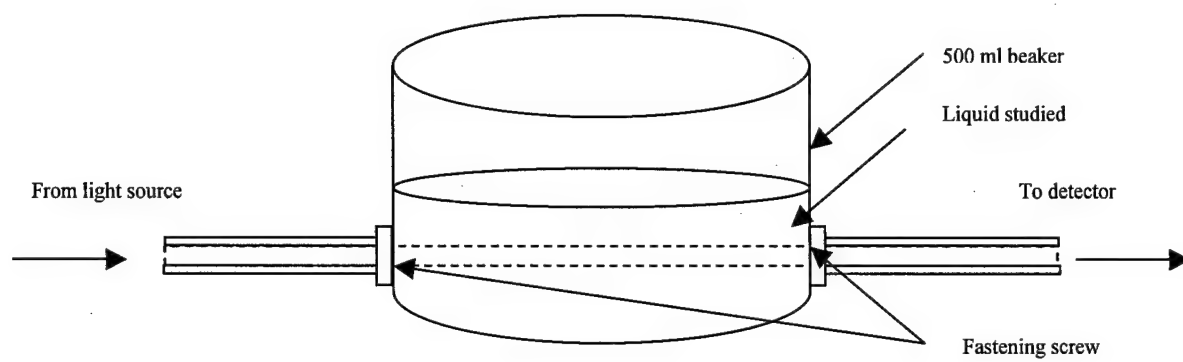
Figure 4.2.3.1 A sketch of the evanescent wave FT-NIR experimental setup.
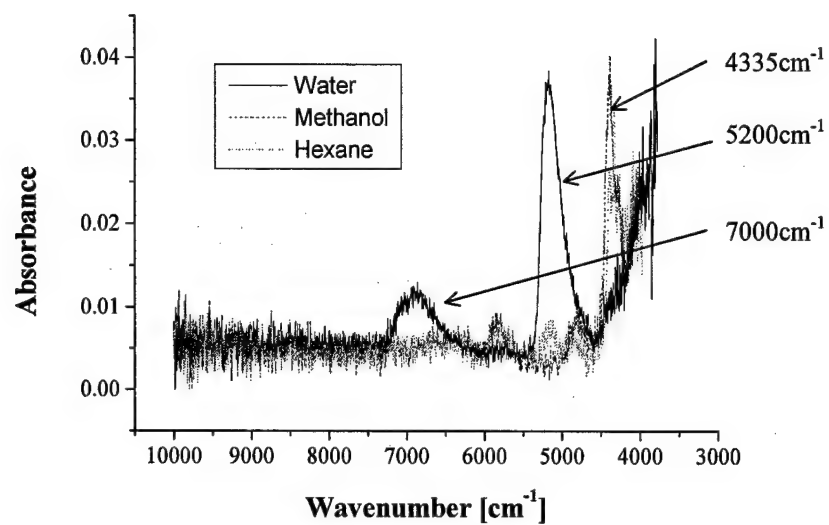
Figure 4.2.3.2 Evanescent wave absorbance spectra of water, methanol and hexane.

4.2.3.2 Tip-to-Tip Mode

To increase the intensity of the NIR signal, a tip-to-tip mode method to collect NIR spectra in situ in adhesive joints is being developed (Figure 4.2.3.3). When light passes through the sample located between the transmitting and the receiving leg of an optical fiber, the sample will selectively absorb some light and the resulting absorbance spectra will reflect the structure of the materials, as shown in Figure 4.2.3.4 and 4.2.3.5. The tip-to-tip NIR configuration can detect chemical reaction in the adhesive joints as well as water absorption.
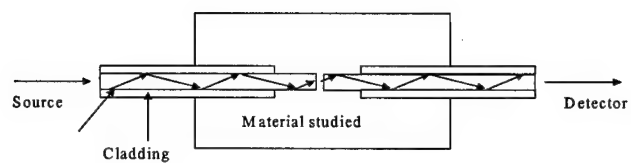
Figure 4.2.3.3 Mechanism of Tip-to-Tip method for NIR measurements.
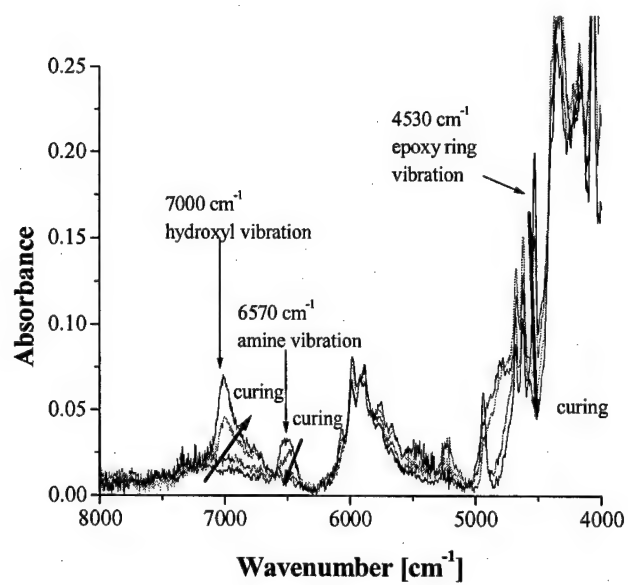
Figure 4.2.3.4 Tip-to-Tip NIR spectra of DGEBA-DETA mixture during cure. The curing procedure consists of three steps: 1) room temperature for 180 min, 2) 60°C for 90min, and 3) 130°C for 60min. In the direction of bold arrows, the spectra were scanned before cure, after the 1st, 2nd and 3rd step of cure, respectively.
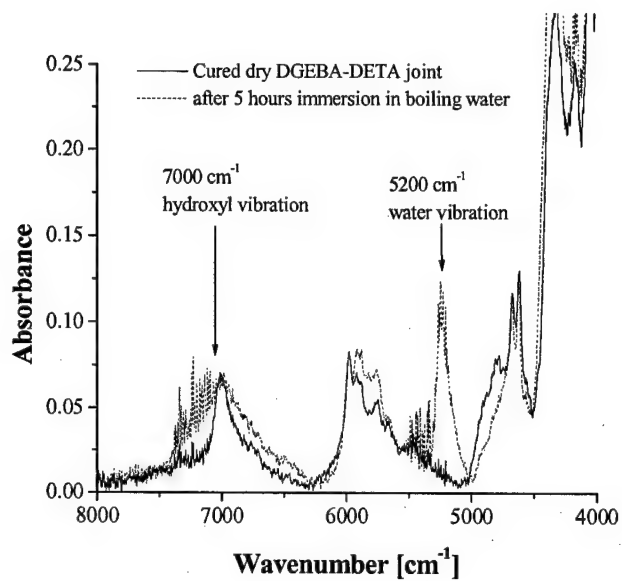
Figure 4.2.3.5 Tip-to-Tip NIR spectra of DGEBA-DETA joint before and after aging in boiling water.

4.2.4 Molecular Dynamics (MD) Study

In section 4.2.1, we reported on our initial molecular dynamics study of water in the DEGBA-DETA system. Those results agreed well with the studies of FT-NIR results. During the past year, we conducted a detailed investigation aimed at understanding the states and dynamics of water in DGEBA-DETA adhesive joints. We used molecular dynamics (MD) simulation to address the following questions: where does water reside within the adhesive (sections 4.2.4.1. and 4.2.4.2.) and how does water move (sections 4.2.4.3., 4.2.4.4. and 4.2.4.5.).

Simulation procedure

Simulations were conducted with Materials Studio (Accelrys Inc.) software. The mixtures of water and a fully reacted epoxy network composed of the stoichiometric amounts of DGEBA and DETA were investigated. The following procedure was employed. First, a polymer network consisting of 25 molecules of DGEBA and 10 molecules of DETA (the stoichiometric ratio) was built. Then, an amorphous cells composed of this polymer network and 0~8%(weight) water molecules were constructed and equilibrated for 50ps prior to the 100ps MD simulation runs.

Results and Discussion

A fragment of the water-containing fully cured network is depicted in Figure 4.2.4.1. Possible hydrogen bonds (HBs) between the absorbed water molecules (shown in bold) and network groups are denoted by dashed lines.
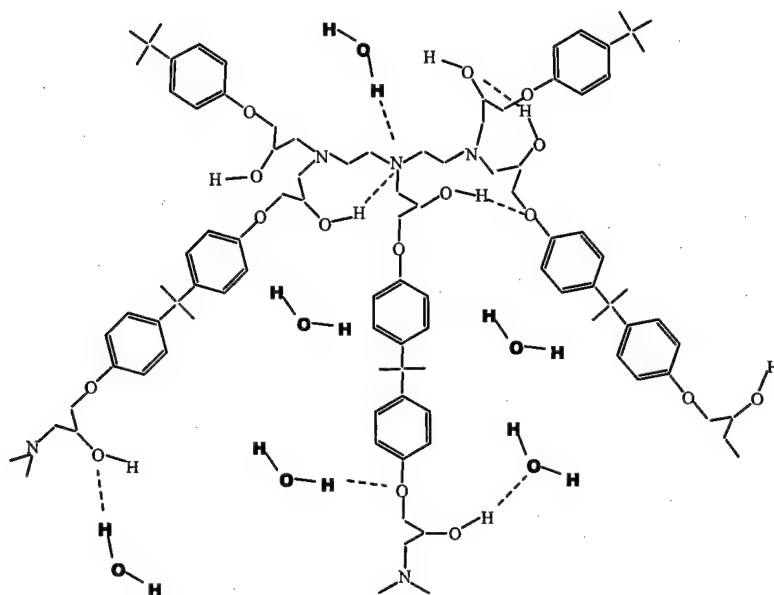
Figure 4.2.4.1 Schematic of a fragment of the chemical structure of the stoichiometric, fully cured water-containing DGEBA-DETA network.

4.2.4.1 "Free" water

The first question we ask is whether water stays in the vicinity of polymer network or exists as "free" water. In this report the designation "free" water refers to those water molecules that never form hydrogen bonds (HBs) with the polymer network within 100ps, i.e. during the time frame of our simulations.

The following two criteria were used in our simulations to designate a hydrogen bond (HB): 1) the distance between hydrogen and an acceptor is less than 2.45Å, and 2) the angle between hydrogen and an acceptor is larger than 145°. Our calculations show that less than 2.5% of the absorbed water is free from HBs with polymer network. This finding is consistent with the experimental results from dielectric relaxation spectroscopy (DRS), and nuclear magnetic resonance (NMR). This implies that, for the moisture content below 8%, the majority of water molecules remain in the vicinity of polymer network polar groups.

4.2.4.2 The nature of hydrogen bonds in dry and moist networks

Epoxy-amine networks have three types of polar groups that can participate in hydrogen bonding; hydroxyl groups, ether groups and tertiary amine groups.

To simplify the description and discussion of our results, we introduce an abbreviated notation for each participant (donor and/or acceptor) in a HB and for all hydrogen bonded pairs. In our two-letter code, the first letter specifies the hydrogen (or the acceptor) atom in a HB, and the second letter characterizes the neighboring atom. As a special case, Hw and Ow are used as symbols for water hydrogen and water oxygen, respectively. Thus HO represent the hydrogen of the network hydroxyl group, OH the

oxygen of the network hydroxyl group, OC the oxygen of the network ether group, NC the nitrogen of the network tertiary amine, Hw the water hydrogen and Ow the water oxygen. A hydrogen bond requires two participating atoms, i.e., a pair. In our notation the hydrogen donor group is always listed first and is separated by a hyphen from the acceptor group. For example, HO-OH defines the hydrogen bond between the hydrogen of a network hydroxyl group (HO) and the oxygen of another network hydroxyl group (OH), while HO-Ow defines the hydrogen bond between the hydrogen of a network hydroxyl group (HO) and a water oxygen (Ow). We also use the symbol n_{HB} to denote the number of hydrogen bonds. All codes used in the text are summarized in Table 4.2.4.1 and we anticipate that a frequent resort to that table will be helpful.

Table 4.2.4.1 MD abbreviations and their description

Code	Description
n_{HB}	Number of hydrogen bonds
HB	Hydrogen bond
HO	Hydrogen atom of hydroxyl groups on the polymer network
Hw	Hydrogen atom of water molecules
NC	Amine atom of tertiary amine groups on the polymer network
OC	Oxygen atom of the ether groups on the polymer network
OH	Oxygen atom of the hydroxyl groups on the polymer network
Ow	Oxygen atom of water molecules
HO-NC	Hydrogen bond between HO and NC
HO-OC	Hydrogen bond between HO and OC
HO-OH	Hydrogen bond between HO and OH
HO-Ow	Hydrogen bond between HO and Ow
Hw-NC	Hydrogen bond between Hw and NC
Hw-OC	Hydrogen bond between Hw and OC
Hw-OH	Hydrogen bond between Hw and OH
Hw-Ow	Hydrogen bond between Hw and Ow

In a dry network, three kinds of HBs are possible. Each of those three HBs involves hydrogen of the network hydroxyl group (HO) and one of the three acceptors: oxygen of the network hydroxyl group (OH), oxygen of the network ether group (OC) or nitrogen of the network tertiary amine (NC). Recall that those HBs are indicated by dashed lines in Figure 4.2.4.1. Our simulation results confirm that all three types of HBs are indeed present. More specifically, of all hydroxyl hydrogens (HO) present in the dry network about 35% (normalized to the maximum value of 100%) form HBs, while the remaining 65% are "free". The 35% HO groups engaged in HBs are distributed as follows (see ordinate, Figure 4.2.4.2): about 26% form HO-OH pairs, 5% form HO-NC pairs and 4% form HO-OC pairs.

In a moist environment, water diffuses into the polymer network. We reiterate that we shall not be principally concerned with the kinetics of moisture absorption and that despite a number of such studies the molecular-level picture of the motions of water molecules and their interactions with the network is far from clear.

Naturally, the absorbed water can form HBs with the network and the next question we ask is: what effect the absorbed water has on the three types of HBs already present in the dry network? The answer is provided in Figure 4.2.4.2, where the number of HBs (n_{HB}) for each of those three pairs is plotted as a function of moisture content. Note that the n_{HB} between the HO-OH pairs decreases with water uptake initially and then levels off at about 3% moisture. It is also interesting to note that the absorbed water in this initial stage (between 0 and 3%) breaks up about one third of the HO-OH HBs present in the dry network. The n_{HB} for the HO-NC and HO-OC pairs does not change appreciably with moisture uptake.
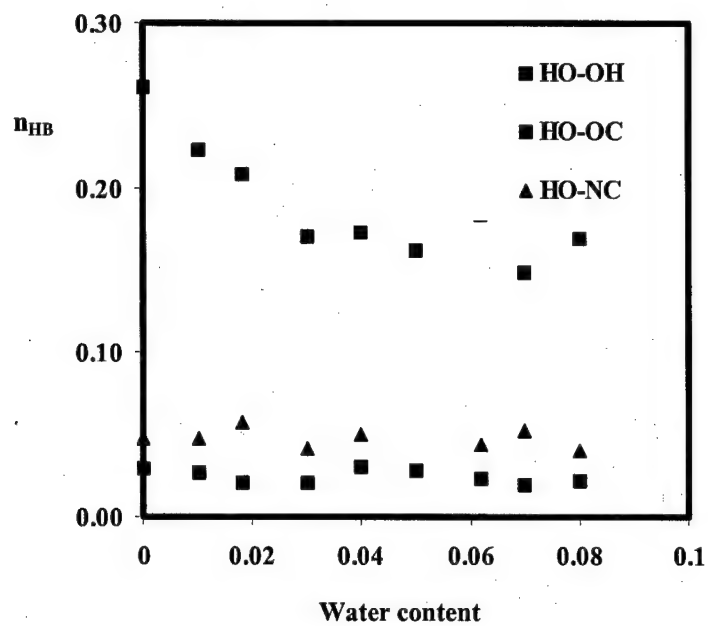
Figure 4.2.4.2 Number of HBs between polar groups of the polymer network as a function of water content. n_{HB} represents an average per hydroxyl hydrogen of the polymer network.

We now take a closer look at the absorbed water molecules and examine in more detail their destination, their location within the network and the type of HBs they form. Towards that goal we calculate the number and the type of HBs in which water hydrogen (Hw) and/or water oxygen (Ow) participate. Those results are shown in Figure 4.2.4.3. as a function of moisture content for five types of HBs. It is apparent that water can form HBs with the network through its oxygen, Ow, (e.g., HO-Ow) and/or its hydrogen, Hw, (e.g., Hw-OH, Hw-OC and Hw-NC), as well as with other water molecules (Hw-Ow). Up to about 4% moisture content, the absorbed water shows preference for hydrogen bonding with the network hydroxyl group (HO-Ow and Hw-OH, filled diamonds and squares, respectively, Figure 4.2.4.3.). The n_{HB} of Hw-OH and HO-Ow pairs that form during that time is about the same. The n_{HB} of Hw-OC and Hw-NC pairs is much smaller and it increases ever so slightly with increasing moisture content. At moisture content in excess of 6%, however, the Hw-Ow HBs become dominant. Nonetheless, when one considers the difference in the concentration between hydroxyl groups of the network and water oxygen (the concentration of the former is ten times that of the latter at the moisture content of 1%), it becomes evident that the preferential hydrogen bonding sequence of Hw is: Ow>OH>NC~OC. Figure 4.2.4.2 and Figure 4.2.4.3 also reveal that the absorbed water breaks up some of the HO-OH HBs in the dry network but also forms HBs with the initially "free" hydroxyl groups (65% in the dry network) and, probably, with a fraction of the broken up HO-OH HBs.

Figure 4.2.4.4. is a composite plot that shows the number of HBs between various network groups, between network and water, and between different water molecules, all as a function of moisture content. All numbers in Figure 4.2.4.4 were

normalized with respect to one hydroxyl group of the polymer network, as opposed to one hydroxyl hydrogen in Figure 4.2.4.2. As a consequence, the initial number of HBs in the dry network in Figure 4.2.4.4 is about twice that in Figure 4.2.4.2 (compare the ordinates in Figure 4.2.4.2 and Figure 4.2.4.4 at 0% moisture), because a hydroxyl group can form HBs through its oxygen *and* its hydrogen. The number of HBs between the network groups decreases with moisture content while the number of HBs between the network and water, and between water molecules increases.
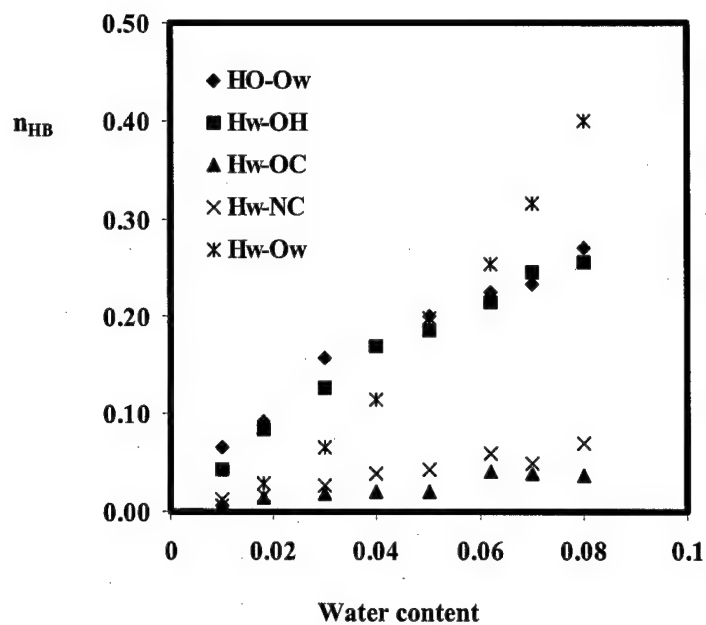
Figure 4.2.4.3 Number of HBs between water and polar groups of the polymer network, and between different water molecules as a function of water content. n_{HB} values are normalized per hydroxyl group of the polymer network.
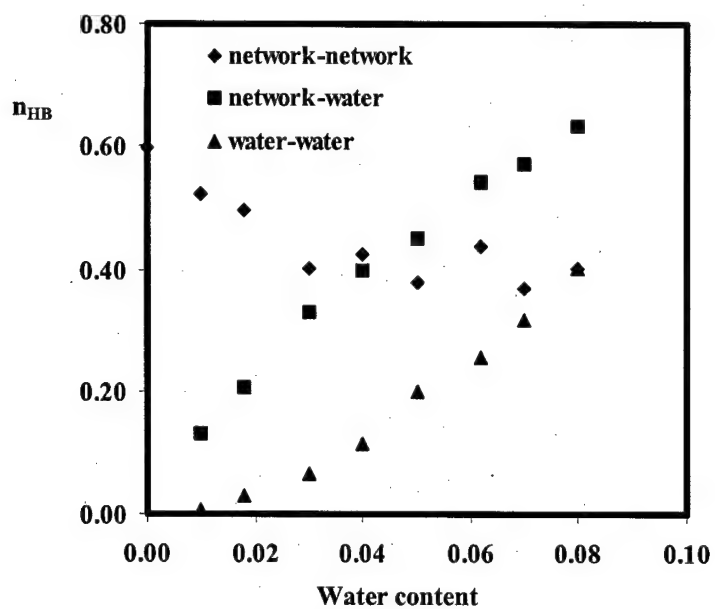
Figure 4.2.4.4 Number of HBs between network polar groups, between water and network polar groups, and between different water molecules as a function of water content. n_{HB} values are normalized per hydroxyl group of the polymer network.

4.2.4.3 Rotational dynamics of water molecules

After learning where water resides, we were interested to find out how water molecules move; freely or in concert with the network group. To accomplish that goal we studied the rotational dynamics of water molecules by tracking the three characteristic vectors that correspond to the principal axes of the water molecule, shown in the inset in Figure 4.2.4.5. The vector that connects the two hydrogen atoms is designated HH; the vector directed along the bisector of the H-O-H bend, which coincides with the direction of the water dipole moment, is designated μ; and the vector perpendicular to the plane of a water molecule is designated $\perp$. We were principally interested in determining the extent to which each of those three vectors at time t retains the orientation it had at time 0. This is mathematically defined by the autocorrelation function for vector orientation, $P(t)$:

Equation 4.2.4.1 $P(t) = <[e(t) \cdot e(0)]>$

where $e(t)$ and $e(0)$ represent the unit vector (HH, μ or $\perp$) at time t and time 0, respectively, and $<>$ denotes the ensemble average over all such vectors.

The time decay of the autocorrelation function to 0.01 is fitted to the well-known Kohlrausch-Williams-Watts (KWW) two-parameter functional form:

Equation 4.2.4.2 $P_{KWW}(t) = \exp[-(t/\tau)^{\beta}]$

where τ is the relaxation time and β the KWW stretch exponential (β_{KWW}).

Figure 4.2.4.5 illustrates the time decay of the autocorrelation function for the three principal vectors (HH, μ and $\perp$).

118

It is very interesting to note that at the end of the 100 ps time interval vectors HH and $\perp$ have no recollection of their orientation at time zero, while vector μ maintains about 50% of its initial orientation. The KWW fits of the autocorrelation function for vectors HH and $\perp$ yielded values of τ_{HH} and $\tau_\perp$ in the range between 2.5-4 ps, independent of the water content. Our simulation of pure liquid water yielded the values for τ_{HH}, $\tau_\perp$ and τ_μ of 2.3, 1.8 and 4.0 ps, respectively, similar to the literature values (2.8, 2.6 and 1.6 ps for τ_{HH}, $\tau_\perp$ and τ_μ respectively). These are interesting findings which suggest that: 1) vectors HH and $\perp$ rotate similarly in pure liquid water and within the polymer network, and 2) the vector μ is slowed down considerably through the interactions with the polymer network. Thus the rotation of water molecules within the network assumes an anisotropic character.

The slowdown in the orientation dynamics of water has been also observed in the aqueous solutions of proteins, micelle, poly(ethylene oxide) and micro emulsions. The obvious question is: what causes this experimentally observed slowdown? One possible explanation lies in the confinement imposed by the surrounding network molecules. But such confinement should be isotropic and hence it is not clear why it would slow down one orientation more than others. An alternative explanation could be sought in the interactions, such as electrostatic and/or hydrogen bonding, between the absorbed water and its surroundings. Since the electrostatic interactions (Coulomb forces) are quite weak compared with HB interaction, we believe that hydrogen bonding is the principal mechanism that drives the observed slowdown of vector μ. In order to confirm this hypothesis we ought to show that: 1) the orientation of polar groups with which

119

water forms HBs is at least as slow, and 2) the HBs between water and network groups are sufficiently stable. Those criteria are discussed in the following sections.

4.2.4.4 The orientation of polar groups of the polymer network

The simulation of the rotational motion of water molecules, described in the previous section, was extended to the polar groups of the polymer network, namely the hydroxyl, the ether and the tertiary amine groups. The analysis was conducted by calculating the autocorrelation function for the following vectors: 1) the vector H-O, connecting the hydroxyl hydrogen with the hydroxyl oxygen; 2) the vector O-C, connecting the ether oxygen with the ether carbon; and 3) the vector N-C, connecting the nitrogen and the neighboring carbon. The autocorrelation function, $P(t)$, is of the same form as eq. 1. Figure 4.2.4.6 illustrate the change in $P(t)$ of those three vectors (H-O, O-C and N-C, respectively) as a function of simulation time with 2% water. The results show that the H-O, O-C and N-C vectors maintain about 60%, 80% and 90%, respectively, of their initial orientation after 100 ps. The implication is clear: the polar groups on the network rotate sufficiently slowly to interact with and slow down the orientation of water. But to attribute the experimentally observed slowdown to interactions with network, the ensuing HBs must be stable over a certain time span, and that is considered next.
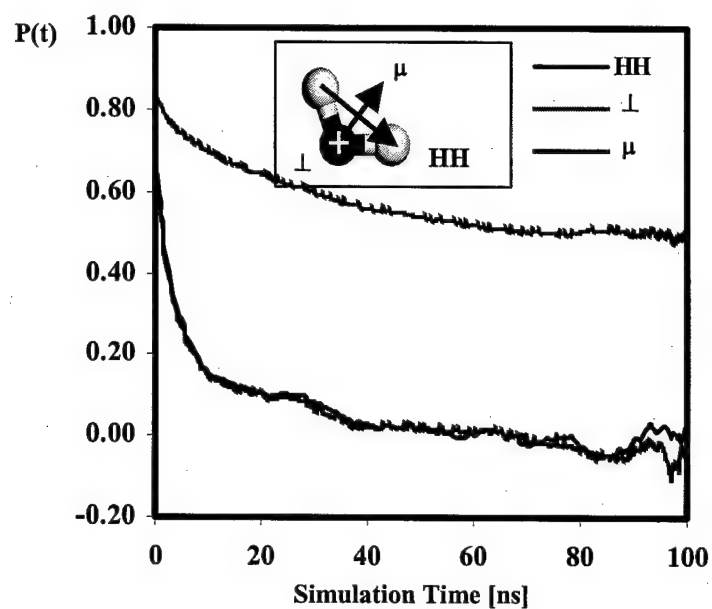
Figure 4.2.4.5 Autocorrelation function of the three characteristic vectors (HH, μ and ⊥) as function of simulation time. Water content is 2% by weight.

4.2.4.5 The dynamics of hydrogen bonds

Now we move on to check whether the HBs are stable enough or not. The time correlation function of HBs was studied following the rationale put forward by Stillinger.[24] The probability that a randomly chosen HB (i.e., donor-acceptor pair) is bonded at time t, provided that the pair was bonded at time t=0 (independent of the possible breakup and reformation in the interim) is described by the time correlation function C(t):

Equation 4.2.4.3 $$C(t) = <h(0)h(t)>/<h^2>$$

where $h(t)$ is a binary function for each HB pair {i, j} of hydrogen (connected to the HB donor group) and the HB acceptor. Then, $h(t) = 1$ if {i, j} are bonded at time t and $h(t) = 0$ if {i, j} are not bonded at time t. The symbol $<>$ denotes an average over all pairs of {i, j} and starting times.

Figure 4.2.4.6 Autocorrelation function of the hydroxyl vector (O-H), ether vector (C-O) and amine vector (N-C) as a function of simulation time.

Figure 4.2.4.7 and Figure 4.2.4.8 show the calculated time correlation function, $C(t)$, for all possible HBs with the HO (Figure 4.2.4.7) and different acceptors, and the Hw (Figure 4.2.4.8) and different acceptors. The water content in Figure 4.2.4.7 and Figure 4.2.4.8 was fixed at 2%, but we hasten to add that analogous results were observed at other water content and hence the data in these two figures depict a general trend. From Figure 4.2.4.7 we learn that there is a 60% probability that hydrogen bonded pairs HO-OH, HO-NC and HO-Ow bonded at time zero (t=0) will remain bonded after 100 ps. The probability that a HO-OC pair bonded at time zero will remain bonded after 100 ps is about 20%; the difference is due to the smaller negative charge of OC in comparison with OH, NC and Ow. Interestingly, the Hw-OH, Hw-NC and Hw-Ow HB pairs bonded at time zero retain only a 20% probability of remaining bonded after 100 ps, as illustrated in Figure 4.2.4.8.. The difference between Figure 4.2.4.7 and Figure 4.2.4.8 could be reconciled by the fact that the translation motion of water is faster than that of the hydroxyl groups. This means that the network groups have higher probability of reforming HBs with previous bonded hydroxyl groups than previously bonded water.

A quantitative comparison of the dynamics of various HB pairs was made by comparing the characteristic relaxation parameters for each pair, τ_R, defined as $c(\tau_R) = e^{-1}$. The results of our calculations, shown in Table 4.2.4.2., are very informative. The key finding is that the characteristic relaxation time for HO-OH, HO-NC and HO-Ow pairs exceeds 100 ps, and hence longer simulation time is needed for a precise calculation of those values. It is important to reiterate that the results displayed in Table 4.2.4.2. did not change with increasing water content (up to 8%) within our simulation time frame of 100 ps.
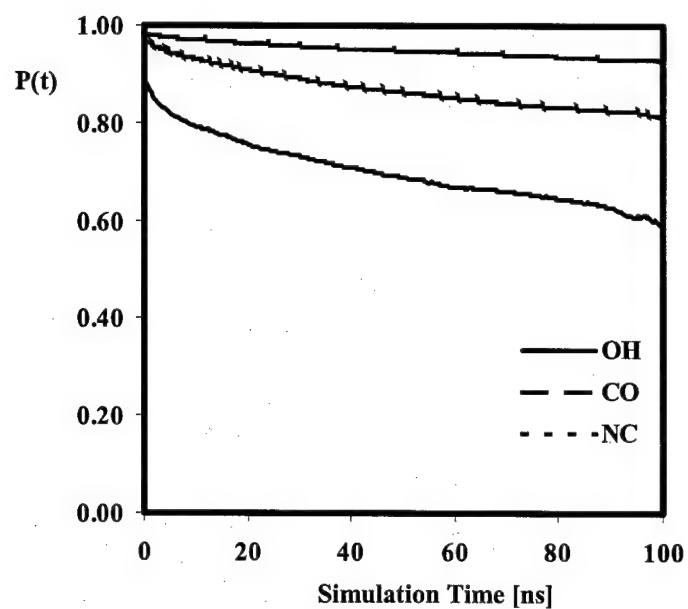
Figure 4.2.4.7   Correlation function, c(t), for HBs of HO with different acceptors as a function of simulation time. Water content is 2% by weight.

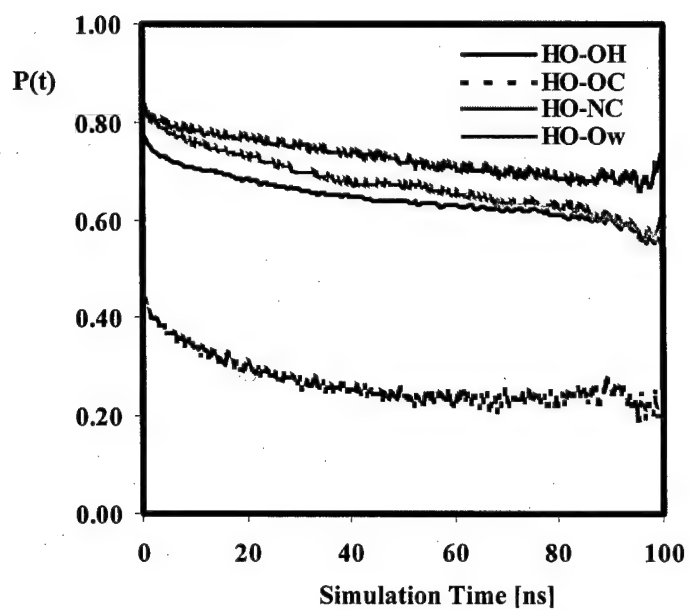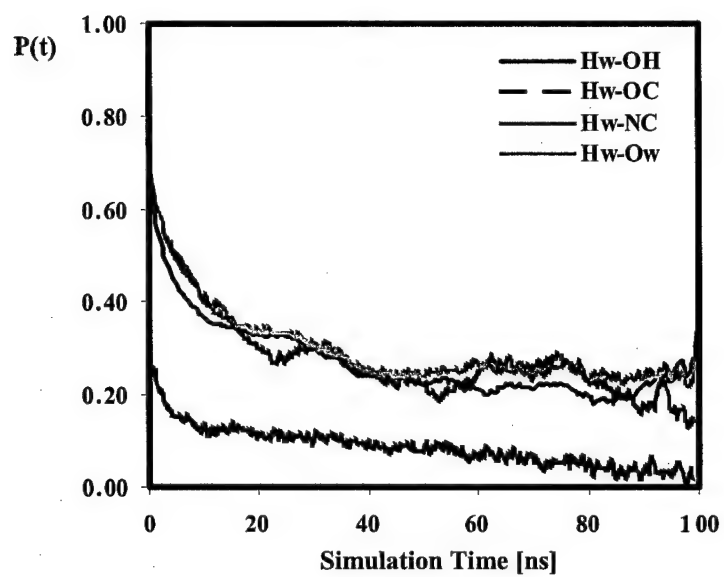Figure 4.2.4.8 Correlation function, c(t,) for HBs of Hw with different acceptors as a function of simulation time. Water content is 2% by weight.

Table 4.2.4.2 MD simulation results: characteristic lifetime, τ_R, of different HBs

HB	HO-OH	HO-OC	HO-NC	HO-Ow	Hw-OH	Hw-OC	Hw-NC	Hw-Ow
τ_R(ps)	>100	~20	>100	>100	~10	~1	~20	~10

The results in Table 4.2.4.2 further suggest that the HO-Ow HB is stable enough to slow down the orientation of water dipole in the direction of its dipole moment μ. The complete picture that emerges from our study regarding the rotation of absorbed water can be summed up as follows: the vectors HH and $\perp$ orient freely, much like in the bulk liquid water, while the vector μ, which coincides with the dipole moment, rotates in concert with the hydroxyl groups of the polymer network. Interesting preliminary results were obtained from the longer time MD simulations that are currently underway in our laboratory. Using simulation time of 10ns and the water content of 3% we find that the relaxation times of the networks hydroxyl groups, the HO-Ow HBs and the vector μ, all have similar time scale of the order of 1 ns. The practically identical time scale of those three motions supports our hypothesis that the water dipole moment rotates with the hydroxyl group of the network. This finding is in excellent agreement with the NMR results of Jelinski, Karasz et al. (Macromolecules 1985, 18, 1091) who report that water absorbed in an epoxy network hops from site to site with an average residence time of 0.7 ns (700ps).

4.3 Comparison between different instruments for DRS

The equipments used, i.e., the α analyzer (1μHz – 3MHz) and HP4291B (1MHz to 1.8GHz), have simpler (and more economic) counterparts, HP4284A (20Hz to 1MHz), and HP8752A (0.3MHz to 1.3GHz), respectively. It was of interest to compare the results obtained using different equipment.

4.3.1 HP4284A vs α analyzer

Figure 4.3.1.1. shows the results obtained on these the two pieces of equipment. Three kinds of samples were used, i.e., a disc-shaped Teflon sheet (a), a disc-shaped joint (b) and a strip-shaped joint (c). It can be seen that in the frequency range (1000Hz-1MHz) the results from the two pieces of equipment agree well, while in the range (20Hz-1000Hz) the result from HP4284A is scattered. The shape of the sample does not influence the reliability of the results.

Figure 4.3.1.1 Comparison between the α analyzer and HP4284A: a) disc-shaped Teflon sample; b) disc-shaped joint sample; c) strip-shaped joint sample.

4.3.2   HP8752A vs HP4291B

Figure 4.3.2.1 shows the results obtained from these two pieces of equipment. Again, three kinds of samples were used: a disc-shaped Teflon patch (a), a disc-shaped joint (b) and a strip-shaped joint (c).

It is seen that for the disc-shaped samples, the results from the two instruments agree well from 1M to 300M Hz. For the strip-shaped sample, the two sets of results agree only in the range between 1M and 20MHz. At higher frequency, the results from HP8752A become unreliable (the permittivity drops to one or less), and at frequency higher than 100M Hz, the results from HP4291B become unreliable (the permittivity drops to one or less).
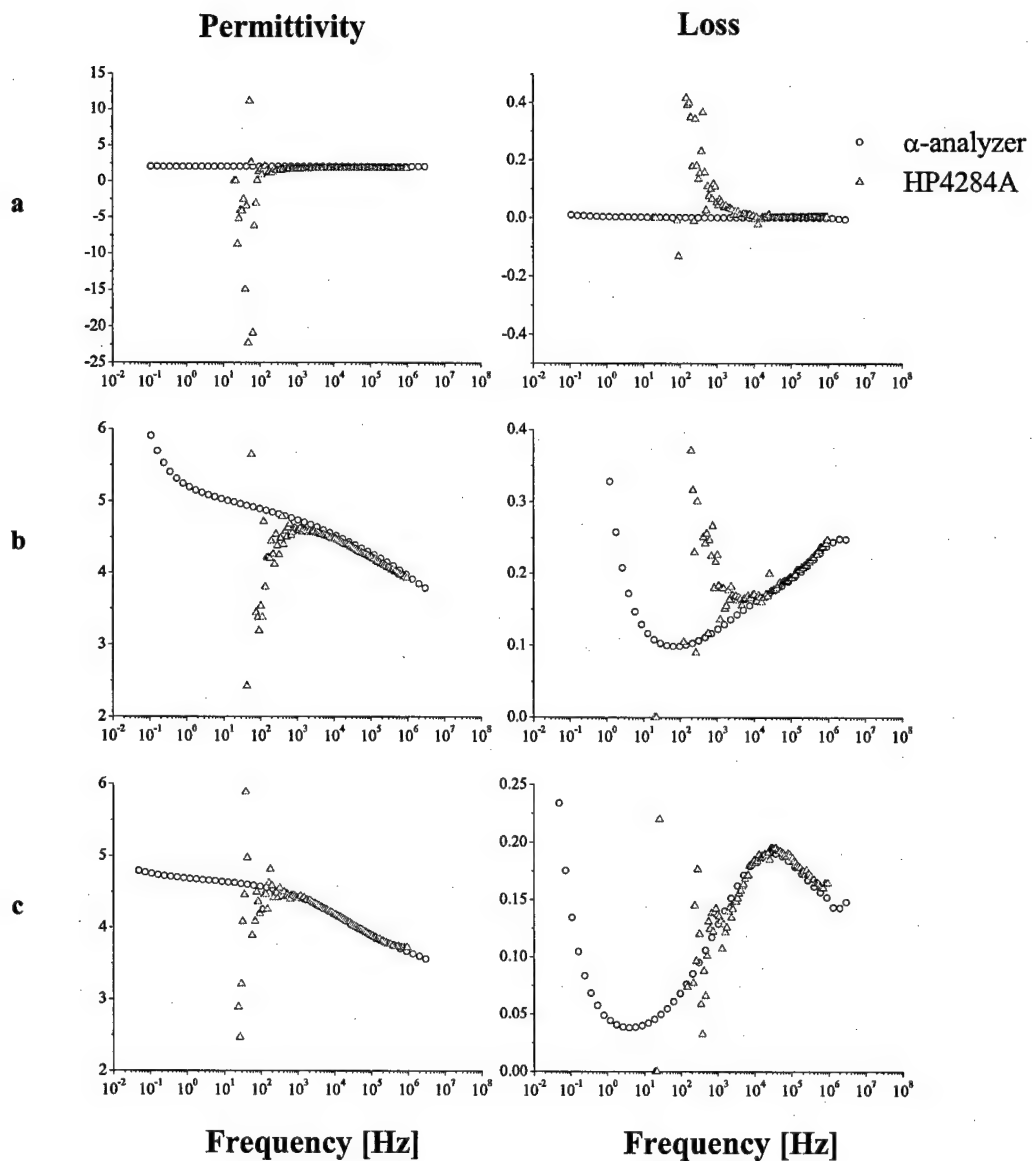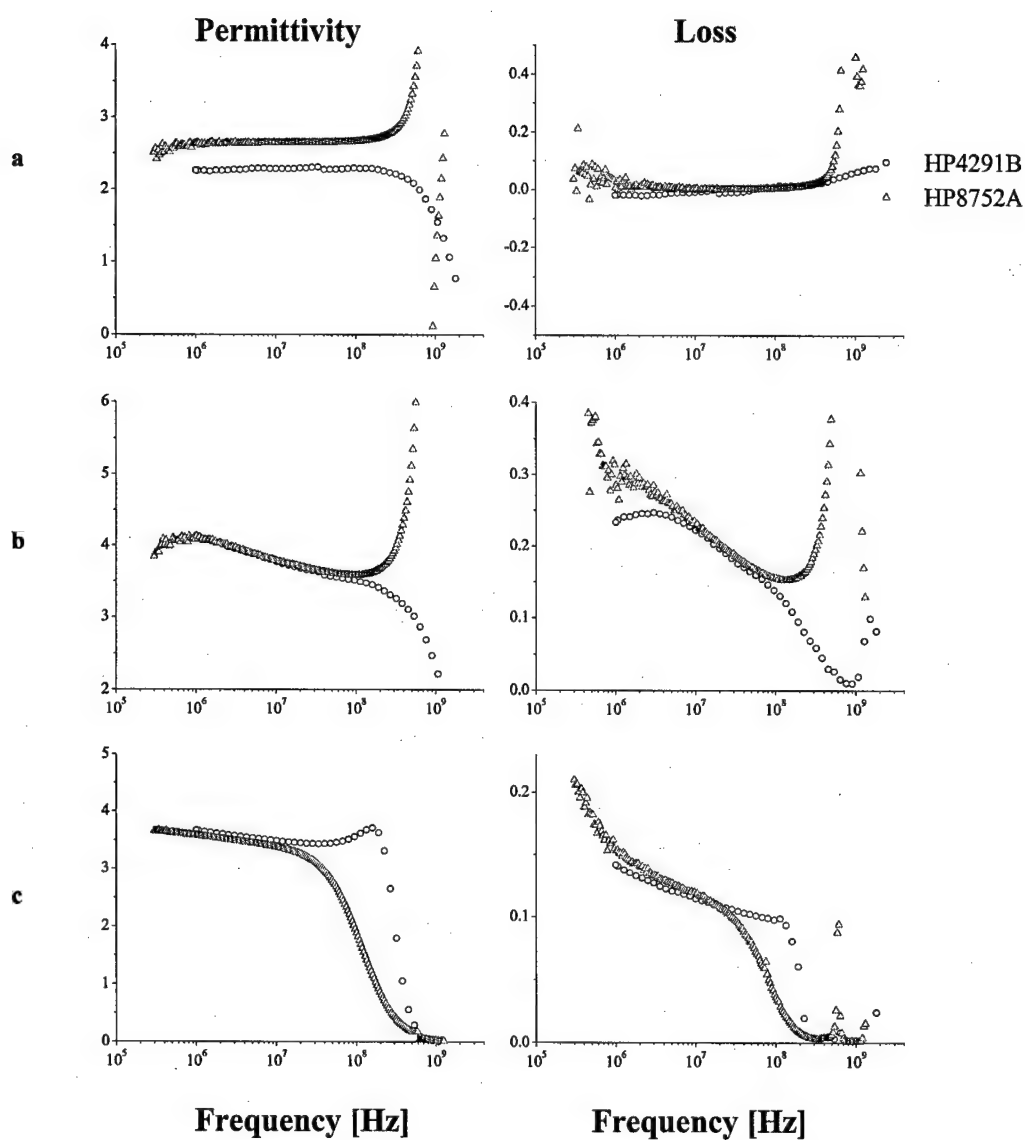
Figure 4.3.2.1 Comparison between HP4291B and HP8752A, a) disc-shaped Teflon sample; b) disc-shaped joint sample; c) strip-shaped joint sample.

References Cited

(1)   Mijovic, J.; Zhang, H. *Macromolecules* **2003**, *36*, 1279.
(2)   Mijovic, J.; Zhang, H. *J. Phys. Chem. B* **2004**, *108*, 2557.
(3)   *HP 8752A/B Network Analyzer Operating Manual*, 1990.
(4)   Weir, M. D.; Bastide, C.; Sung, C. S. P. *Macromolecules* **2001**, *34*, 4923.
(5)   Starr, F. W.; Nielsen, J. K.; Stanley, H. E. *Phys. Rev. Lett.* **1999**, *82*, 2294.

(6)   Matsumoto, M.; Saito, S.; Ohmine, I. *Nature* **2002**, *416*, 409.
(7)   Smith, G. D.; Bedrov, D.; Borodin, O. *Phys. Rev. Lett.* **2000**, *85*, 5583.
(8)   Yarovsky, I.; Evans, E. *Polymer* **2002**, *43*, 963.
(9)   Sides, S. W.; Grest, G. S.; Stevens, M. J. *Macromolecules* **2002**, 566.
(10)   Berndt, K. D.; Güntert, P.; Wüthrich, K. *J. Mol. Biol.* **1993**, *234*, 735.
(11)   Zhang, H.; Mijovic, J. *Macromolecules* **2004**, *37*, 5844.
(12)   Noda, I. *Bull. Am. Phys. Soc.* **1986**, *31*, 520.
(13)   Noda, I. *Appl. Spectrosc.* **1993**, *47*, 1329.
(14)   Jung, Y. M.; Czarnik-Matusewicz, B.; Ozaki, Y. *J. Phys. Chem. B* **2000**, *104*, 7812.
(15)   Liu, M.; Wu, P.; Ding, Y.; Chen, G.; Li, S. *Macromolecules* **2002**, *35*, 5500.
(16)   Musto, P. *Macromolecules* **2003**, *36*, 3210.
(17)   Wu, P.; Yang, Y.; Siesler, H. W. *Polymer* **2001**, *42*, 10181.
(18)   Chae, B.; Lee, S. W.; Ree, M.; Jung, Y. M.; Kim, S. B. *Langmuir* **2003**, *19*, 687.
(19)   He, Y.; Wang, G.; Cox, J.; Geng, L. *Anal. Chem.* **2001**, *73*, 2302.
(20)   Eads, C. D.; Noda, I. *J. Am. Chem. Soc.* **2002**, *124*, 1111.
(21)   Dowell, N. G.; Ashbrook, S. E.; McManus, J.; Wimperis, S. *J. Am. Chem. Soc.* **2001**, *123*, 8135.
(22)   Noda, I. In *Handbook of vibrational spectroscopy*; Griffiths, P. R., Ed.; John Wiley & Sons: Chichester, 2002; Vol. 3, pp 2123-2134.
(23)   Ozaki, Y. In *Handbook of vibrational spectroscopy*; Griffiths, P. R., Ed.; John Wiley & Sons: Chichester, 2002; Vol. 3, pp 2135-2172.
(24)   Stillinger, F. H. *Adv. Chem. Phys.* **1975**, *31*, 1.

5 Personnel Supported

1. Jovan Mijovic, Professor of Chemical Engineering

2. Hua Zhang, PhD candidate in Chemical Engineering

6 Publications

1. Zhang, H., Mijovic, J. "Using Two-Dimensional Dielectric Relaxation Spectroscopy (2D-DRS) to Study the Effect of Water on the Dynamics of Epoxy-Amine Networks", *Macromolecules* **2004**, 37, 5844.

2. Mijovic, J., Zhang, H. "Molecular Dynamics Simulation Study of Motions and Interactions of Water in a Polymer Network", *J. Phys. Chem. B.* **2004**, 108, 2557.

3. Mijovic, J., Zhang, H. "Local Dynamics and Molecular Origin of Polymer Network-Water Interactions as Studied by Broadband Dielectric Relaxation Spectroscopy, FTIR and Molecular Simulations", *Macromolecules* **2003**, 36, 1279.

4. Mijovic, J., Miura, N., Zhang, H. "Local Dynamics of Bismaleimide Adhesives in an Aggressive Environment", *J. Adhesion* 2001, 77, 323.

7 Presentations

1. Mijovic, J.; Zhang, H. "Experimental and simulation study of interactions between absorbed water and a thermoset network", presented at the 2nd International Mijovic, J.; Zhang, H. "The Origin and Dynamics of Water-

Networks Interactions in Adhesives Joints", presented at 2nd International Conference on Times of Polymers, Ischia, Naples, Italy, June, 2004.

2. Mijovic, J.; Zhang, H. "Dielectric Spectroscopy as a Non-Destructive Inspection Tool to Assess the States of Adhesives", presented at AFOSR Polymer Matrix Composite Polymer Review, Long Beach, CA, May, 2004.

3. Zhang, H.; Mijovic, J. "Understanding the Interaction between Polymer Network-Water on the Molecular Level", presented at the 27th Annual Meeting of the Adhesion Society, Wilmington, NC, Feb. 2004.

4. Zhang, H.; Mijovic, J. "Understanding Polymer Network- Water Interactions— with Broadband Dielectric Relaxation Spectroscopy, FTIR and Molecular Simulations", presented at the American Chemical Society National Meeting, New York, NY, Sep., 2003.

5. Zhang, H.; Mijovic, J. "Environmental Effects on Polymers, Composites and Adhesives used in the Aerospace Industry", presented at the International Workshop on Corrosion in Aircraft Structures and Ground Vehicles, Ravello, Italy, April, 2003.

6. Zhang, H.; Mijovic, J. "Dielectric Relaxation Spectroscopy and Molecular Dynamics Study of Polymer Network-Water Interactions", presented at 26th Annual Meeting of the Adhesion Society, Myrtle Beach, Feb., 2003.

7. Mijovic, J.; Zhang, H. "Experimental and simulation study of interactions between absorbed water and a thermoset network", presented at the 2nd International Conference on Broadband Dielectric Spectroscopy and its Applications, September 2-6, 2002, Leipzig, Germany.

8. Mijovic, J.; Zhang, H. "Dielectric spectroscopy as a non-destructive inspection (NDI) tool to assess aging of adhesively bonded structures", presented at the International Conference on Times of Polymers (TOP), October 20-23, 2002, Ischia, Italy.

9. Zhang, H.; Mijovic, J. "Dynamics of water-network interactions by DRS and FTIR", presented at the Eastern Analytical Symposium, November 14-17, 2002, Somerset, NJ.

10. Mijovic, J.; Zhang, H. "Local dynamics and molecular origin of polymer network-water interactions as studied by broadband dielectric relaxation spectroscopy, FTIR and molecular simulations", presented at the 26th Annual Meeting of The Adhesion Society, February 23-26, 2003, Myrtle Beach, SC. Published in The Proceedings of The 26th Annual Meeting of The Adhesion Society, pp. 328-330.

11. Mijovic, J.; Zhang, H. "Environmental effects on polymers, adhesives and composites in aerospace applications", presented at the International Workshop on Corrosion in Aircraft Structures and Ground Vehicles", April 14-16, 2003, Ravello, Italy.

8 Inventions or patent disclosures

None at present